1521-0111/106/1/56–70$35.00
MOLECULAR PHARMACOLOGY

dx.doi.org/10.1124/molpharm.124.000881
Mol Pharmacol 106:56–70, July 2024

Allosteric Inhibition and Pharmacochaperoning of the Serotonin Transporter by the Antidepressant Drugs Trazodone and Nefazodone

Ali El-Kasaby, Danila Boytsov, Ameya Kasture, Günther Krumpl, Thomas Hummel, Michael Freissmuth, and Walter Sandtner

Institute of Pharmacology and the Gaston H. Glock Research Laboratories for Exploratory Drug Development, Centre of Physiology and Pharmacology (A.E.-K., D.B., M.F., W.S.), Medical University of Vienna, Vienna, Austria; Department of Neurobiology, University of Vienna, Vienna, Austria (A.K., T.H.); and MRN Medical Research Network GmbH, Vienna, Austria (G.K.)

Received January 23, 2024; accepted May 7, 2024

ABSTRACT

The antidepressants trazodone and nefazodone were approved some 4 and 3 decades ago, respectively. Their action is thought to be mediated, at least in part, by inhibition of the serotonin transporter [SERT/solute carrier (SLC)-6A4]. Surprisingly, their mode of action on SERT has not been characterized. Here, we show that, similar to the chemically related drug vilazodone, trazodone and nefazodone are allosteric ligands: trazodone and nefazodone inhibit uptake by and transport-associated currents through SERT in a mixed-competitive and noncompetitive manner, respectively. Contrary to noribogaine and its congeners, all three compounds preferentially interact with the Na^+-bound outward-facing state of SERT. Nevertheless, they act as pharmacochaperones and rescue the folding-deficient variant SERT-P601A/G602A. The vast majority of disease-associated point mutations of SLC6 family members impair folding of the encoded transporter proteins. Our findings indicate that their folding defect can be remedied by targeting allosteric sites on SLC6 transporters.

SIGNIFICANCE STATEMENT

The serotonin transporter is a member of the solute carrier-6 family and is the target of numerous antidepressants. Trazodone and nefazodone have long been used as antidepressants. Here, this study shows that their inhibition of the serotonin transporter digressed from the competitive mode seen with other antidepressants. Trazodone and nefazodone rescued a folding-deficient variant of the serotonin transporter. This finding demonstrates that folding defects of mutated solute carrier-6 family members can also be corrected by allosteric ligands.

Introduction

The three transporters for the monoamines norepinephrine [NET/solute carrier (SLC)-6A2], dopamine (DAT/SLC6A3), and serotonin (SERT/SLC6A4) are closely related. They share a rich pharmacology, i.e., several hundred compounds are known to bind to these three transporters with variable selectivity (Sitte and Freissmuth, 2015). Ligands can act as typical and atypical inhibitors or as full and partial substrates/releasers (Bhat et al., 2019). Trazodone, nefazodone, and vilazodone are inhibitors of the serotonin transporter. However, their antidepressant action differs from that of selective serotonin reuptake inhibitors. Vilazodone has been classified as a SPARI (selective partial agonist and reuptake inhibitor) because it is an inhibitor of the serotonin transporter and it elicits a partial agonistic activity at 5-HT_{1A}-receptors (Heinrich et al., 2004; Dawson and Watson, 2009). Trazodone and nefazodone are chlorophenylpiperazines, which are classified as serotonin antagonists and reuptake inhibitors because they inhibit SERT and block $5HT_{2A}$ and $5HT_{1A}$ receptors (Cusack et al., 1994; Owens et al., 1997; Tatsumi et al., 1997). However, trazodone, in particular, also has appreciable affinity for α-adrenergic receptors (Krege et al., 2000).

SERT harbors two binding sites: 1) a central binding site, which is referred to as S1, accommodates the substrate serotonin and the cosubstrate ions, i.e., two sodium ions and one chloride ion, and 2) in addition, there is a vestibular binding site (referred to as S2), which is allosterically linked to the central binding site (Coleman et al., 2016; Zhu et al., 2016). Typical inhibitors bind to the S1 site of monoamine transporters and trap them in the outward-facing conformation. Atypical inhibitors stabilize conformations other than the outward-facing conformation. This is of interest because there is a

This work was supported by grants from the Vienna Science and Technology Fund/WWTF [Grant LSC17-026] (to M.F.), from the AOP foundation (to M.F.), and from Austrian Science Fund/FWF [Grant P31813] (to W.S.).
The authors declare no competing interest.
[1]A.E.-K. and D.B. contributed equally to this work.
dx.doi.org/10.1124/molpharm.124.000881.

ABBREVIATIONS: CI, confidence interval; DAT, dopamine transporter; ER, endoplasmic reticulum; FB, fan-shaped body; k_{on}, association rate constant; k_{off}, dissociation rate constant; RRID, research resource identifier; mCPP, *meta*-chlorophenylpiperazine; NET, norepinephrine transporter; SERT, serotonin transporter; SLC, solute carrier; TRH, tryptophan hydroxylase; UAS, upstream activating sequence; YFP, yellow fluorescent protein.

growing list of mutations that cause misfolding of SLC6 family members (Freissmuth et al., 2018) and other solute carriers (Bhat et al., 2021a) and thus give rise to human diseases. Due to their different binding mode, atypical inhibitors can act as pharmacochaperones (Bhat et al., 2019): their binding to folding intermediates and/or their stabilization of the inward-facing state allows correcting the folding defect and restoring endoplasmic reticulum (ER) export, cell surface delivery, and transport activity of mutated solute carriers.

SERT is the most extensively studied solute carrier (César-Razquin et al., 2015; Schlessinger et al., 2023). This is also true for ER export and folding of SERT, which have been examined in great detail (El-Kasaby et al., 2010, 2014; Sucic et al., 2011; Sucic et al., 2013; Koban et al., 2015; Bhat et al., 2017, 2020, 2023; Ponleitner et al., 2022). Vilazodone was found to reside in this S2 binding site of SERT and, accordingly, to act as an allosteric, noncompetitive inhibitor (Plenge et al., 2021). Trazodone and nefazodone were approved as antidepressants some 4 and 3 decades ago, respectively. Nevertheless, surprisingly, their mode of SERT inhibition has never been investigated. Trazodone, nefazodone, and vilazodone are related in structure. Here, we surmised that, because of their similar structures, these three compounds shared a similar mechanism of action on SERT, which differed from those of typical inhibitors. We show that vilazodone and trazodone are mixed-competitive inhibitors and that nefazodone blocks substrate uptake by SERT noncompetitively. Importantly, all three compounds and *meta*-chlorophenylpiperazine (mCPP; a metabolite of trazodone and nefazodone) rescued SERT-P601A/G602A, a severely misfolded variant (El-Kasaby et al., 2014), in cells and in fly brain, demonstrating that they can act as pharmacochaperones.

Materials and Methods

Materials. Vilazodone hydrochloride (SML1098), trazodone hydrochloride (T6154), and cycloheximide (239763) were purchased from Sigma Aldrich (St. Louis, MO), and mCPP (*meta*-chlorophenylpiperazine) hydrochloride (B5027) was purchased from APExBIO (Houston, TX). [^{3}H]5-HT (37.5 Ci/mmol) and [^{3}H]citalopram (80.8 Ci/mmol) were purchased from PerkinElmer Life Sciences (Waltham, MA). Scintillation fluid (Rotiszint eco plus) was purchased from Carl Roth GmbH (Karlsruhe, Germany). Anti-GFP antibody [rabbit, ab290; research resource identifier (RRID): AB_2313768] was from Abcam (Cambridge, UK). An antibody raised against an N-terminal peptide of the G protein β subunit was used to verify comparable loading of lanes (Hohenegger et al., 1996). The secondary antibody (Donkey anti-rabbit, IRDye 680RD; RRID: AB_2716687) was obtained from LI-COR Biotechnology GmbH (Bad Homburg, Germany). Cell culture media and antibiotics were obtained from Capricorn Scientific GmbH (Ebsdorfergrund, Germany) and InvivoGen (San Diego, CA), respectively. All other chemicals were of analytical grade and were obtained from Sigma-Aldrich.

Cell Culture. HEK293 cells were purchased from the American Type Culture Collection (CRL-1573, American Type Culture Collection, Manassas, VA; RRID: CVCL_0045) and authenticated by short tandem repeats profiling at the cell culture core facility of the Medical University of Graz, Austria. The cells were cultured in Dulbecco's modified Eagle's medium supplemented with 10% heat-inactivated fetal bovine serum, 60 mg L^{-1} penicillin, 100 mg L^{-1} streptomycin, and 5 mg L^{-1} plasmocin. HEK293 cells expressing GFP-tagged SERT, which were used for patch-clamp experiments, were cultured in a medium supplemented with 150 mg L^{-1} of zeocin and 6 mg L^{-1} blasticidin. The expression of GFP-SERT was induced by 1 mg L^{-1} of tetracycline 24 hours prior to electrophysiology. HEK293 cells stably expressing yellow fluorescent protein (YFP)-tagged SERT, which were used for uptake and immunoblotting experiments, were cultured in medium supplemented with 50 μg mL^{-1} of geneticin (G418) to maintain selective pressure. All cells were regularly tested for mycoplasma contamination by 4′,6-diamidino-2-phenylindole staining. All antibiotics were purchased from InvivoGen.

Uptake of [^{3}H]5-HT. HEK293 cells stably expressing either YFP-tagged wild-type human SERT or SERT-P601A/G602A were seeded on either in poly-D-lysine–coated 48-well (10^5 cells/well) or 96-well plates (2×10^4 cells/well) for the determination of K_M and V_{max} of 5-HT transport and for uptake inhibition, respectively. Cells were allowed to adhere for 24 hours. Thereafter, the medium was removed, and cells were washed twice with Krebs-HEPES buffer (10 mM HEPES·NaOH, pH 7.4; 120 mM NaCl; 3 mM KCl; 2 mM $CaCl_2$; 2 mM $MgCl_2$; and 2 mM glucose). The K_M and V_{max} of substrate uptake was determined by incubating the cells for 1 minute in a final volume of 0.1 mL containing [^{3}H]5-HT concentrations ranging from 0.2 to 20 μM (specific activity progressively diluted from 40 cpm/fmol to 400 cpm/pmol) in the absence and presence of cocaine (5 μM; as a reference compound for competitive inhibition), vilazodone (1, 3, and 10 μM), trazodone (1, 3, and 10 μM), nefazodone (5, 10, 30, and 100 μM), or mCPP (1, 3, and 10 μM). The IC_{50} of inhibitors was determined in 0.1 mL buffer containing carrier-free 0.1 μM [^{3}H]5-HT; inhibitors were either added simultaneously with substrate, or cells were allowed to preincubate for 15 minutes in the presence of the inhibitors. Nonspecific uptake was defined in the presence of 10 μM paroxetine. Uptake reactions were terminated after 1 minute by aspiration of the reaction buffer followed by two rapid washes with ice-cold Krebs-HEPES buffer. Subsequently, cells were lysed with 1% SDS to release the retained radioactivity, which was quantified by liquid scintillation counting.

Pharmacochaperoning Experiments. HEK293 cells stably expressing SERT-P601/G602A were seeded in poly-D-lysine–coated 24-well plates (2×10^5 cells/well) or 48-well plates for incubation in cell culture medium containing vilazodone and of the other compounds (i.e., trazodone, nefazodone, and mCPP), respectively. Control incubations were done in cell culture medium alone. After 24 hours at 37°C, the medium was aspirated. Cells, which had been preincubated with vilazodone, were incubated seven times for 10 minutes in the presence of 2 ml cow milk (ultrahigh-temperature homogenized milk containing 3.5% fat, 2.3% fatty acid, 4.8% sugar, and 3.3% protein) or buffer. After these incubations, the cells were washed twice with 2 ml Krebs-HEPES buffer. Cells, which had been incubated with trazodone, nefazodone, or mCCP, were washed five times with 1 ml of Krebs-HEPES buffer. Thereafter, substrate uptake was performed as outlined above in the presence of 0.1 μM [^{3}H]5-HT in an incubation volume of 0.2 mL and of 0.1 mL for vilazodone and for the other compounds, respectively.

Alternatively, HEK293 cells stably expressing YFP-tagged SERT-P601/G602A were seeded on six-well plates (1×10^6 cells/dish) and incubated in the absence and presence of vilazodone, trazodone, nefazodone, or mCPP. After 24 hours, cells were washed thrice with ice-cold PBS, detached by mechanical scraping, and harvested by centrifugation at 1000*g* for 5 minutes. The cell pellet was lysed in a buffer containing Tris·HCl, pH 8.0; 150 mM NaCl; 1% dodecyl maltoside; and 1 mM EDTA and protease inhibitors (Complete, Roche Applied Science). The detergent-insoluble material was removed by centrifugation (16,000*g* for 15 minutes at 4°C). Aliquots of the soluble supernatant were used to assess the level of core-glycosylated, ER-resident SERT-P601/G602A of transporters harboring mature glycans by immunoblotting. Lysates were also prepared from cells stably expressing YFP-tagged SERT.

Membrane Preparation and [^{3}H]Citalopram Binding. Membranes were prepared from HEK293 cells stably expressing GFP-SERT. The cells were washed twice with PBS, mechanically detached, and harvested by centrifugation at 2000 rpm for 10 minutes. The pellets were resuspended in buffer containing 20 mM Tris HCl, pH 7.4, and 2 mM $MgCl_2$, and the suspension was frozen in liquid nitrogen.

After two freeze-thaw cycles, the suspension was sonicated three times for 10 seconds on ice with 30-second intervals. Membranes were harvested by centrifugation at 40,000*g* for 15 minutes, and the pelleted membranes were resuspended in the same buffer and frozen in liquid nitrogen. The protein concentration was estimated with the Bio-Rad protein assay dye reagent (Bio-Rad; Hercules, CA). The binding reaction (0.1 mL final volume) was done in the presence of 3–5 nM [^{3}H]citalopram and increasing, logarithmically spaced concentrations of inhibitors in buffer containing either high concentrations of either Na^+ (20 mM Tris.HCl, pH 7.4; 2 mM $MgCl_2$; and 120 mM NaCl) or of K^+ (20 mM Tris HCl, pH 7.4; 2 mM $MgCl_2$; 4 mM NaCl; and 120 mM KCl) and about 2.5 μg or 30 μg of membranes, respectively. Nonspecific binding was measured in the presence of 10 μM paroxetine. After an incubation for 60 minutes at 22°C, the binding reaction was terminated by filtration over polyethylenimine (0.5%) precoated glass fiber filters (GF/B), which were washed with ice-cold wash buffer (10 mM Tris·HCl, pH 7.4; 120 mM NaCl; and 2 mM $MgCl_2$). The radioactivity trapped on the filters was quantified by liquid scintillation counting.

Immunoblotting. Aliquots of detergent lysates (30 μg), which had been prepared as outlined above, were dissolved in Laemmli sample buffer containing 1% SDS and 20 mM DTT, denatured at 45°C for 30 minutes, and resolved by denaturing polyacrylamide gel electrophoresis. The resolved proteins were transferred onto nitrocellulose membranes, which were incubated overnight with an antibody against GFP (rabbit, ab290; diluted 1:5000 in 20 mM Tris.HCl, pH 7.4; 150 mM NaCl; and 0.1% Tween20). The immunoreactive bands were visualized by fluorescence detection using a donkey anti-rabbit secondary antibody at 1:5000 dilution (IRDye 680RD, LICOR). The lower part of the blot was also probed with the antibody recognizing the G protein β subunits to verify equal loading.

Whole-Cell Patch-Clamp Recordings. HEK293 cells stably expressing wild-type GFP-tagged human SERT were seeded at low density on Petri dishes coated with poly-D-lysine. Twenty hours later, these cells were subjected to patch-clamp recordings in the whole-cell configuration using Axon 200B amplifier (RRID: SCR_018866) equipped with Axon 1550 digitizer (Molecular Devices, LLC, San José, CA). The cells were continuously maintained in an external solution containing 150 mM NaCl, 3 mM KCl, 2.5 mM $CaCl_2$, 2 mM $MgCl_2$, 20 mM glucose, and 10 mM HEPES (pH adjusted to 7.4 with NaOH), and the drugs were diluted therein. The internal solution in the patch pipette contained 150 mM K-MES, 1 mM $CaCl_2$, 0.7 mM $MgCl_2$, 10 mM HEPES, and 10 mM EGTA (pH adjusted to 7.2 with KOH). Drugs were applied using a perfusion system (Octaflow II; ALA Scientific Instruments, Inc., Farmingdale, NY), allowing for complete solution exchange around the cells within 50 milliseconds. All experiments were conducted at 25°C with precise temperature control. This was achieved with a temperature control unit (cell microcontrol inline preheater; Green Leaf Scientific, Dublin, Ireland), which was linked to a temperature control system (PTC-20; npi electronic GmbH, Tamm, Germany). For positioning the patch-clamp pipette and the perfusion system, we used PatchStar micromanipulators (Scientifica Ltd., Uckfield, UK; RRID: SCR_018405). Recordings were sampled at 10 kHz. Current amplitudes and associated kinetics were quantified using Clampfit software (Molecular Devices; RRID: SCR_011323). Passive holding currents were subtracted, and the traces were filtered using a 100-Hz digital Gaussian low-pass filter.

Drosophila Genetics and Drug Treatment. Previously generated transgenic upstream activating sequence (UAS) reporter lines for YFP-tagged human wild-type SERT and SERT-P601A/G602A were used (Bhat et al., 2020). Tryptophan hydroxylase (TRH)-T2A-Gal4 (Bloomington stock no. 84694; Bloomington Drosophila Stock Center, Bloomington, IN; RRID: BDSC_84694) was used to drive the expression of transporters in serotonergic neurons. Three-day-old male TRH-T2A-Gal4/UAS-YFP-hSERT wild type or TRH-T2A-Gal4/UAS-YFP-hSERT-PG601,602AA flies were treated with food supplemented with 100 μM trazodone, 100 μM vilazodone, 100 μM nefazodone, or 100 μl DMSO for 48 hours. Adult fly brain images were captured by confocal microscopy (Leica SP5). All fly lines were kept at 25°C, and all crosses were performed at 25°C.

Immunohistochemistry and Imaging. Adult fly brains were dissected in PBS and fixed in 2% paraformaldehyde in PBS for 1 hour at room temperature. Brains were then washed three times in 0.1% Triton X-100 in PBS for 20 minutes on a shaker. Blocking was performed in 10% goat serum for 1 hour at room temperature on a shaker. Brains were then incubated in primary antibody overnight in PBS containing 3% bovine serum albumin and 0.3% Triton X-100 at 4°C on a shaker. The rabbit polyclonal IgG directed against GFP (1:1000 dilution; A-11122, Invitrogen) was used as primary antibodies. After three washes for 20 minutes with PBS containing 0.1% Triton X-100, the brains were incubated overnight at 4°C with a secondary antibody in PBS containing 0.3% Triton X-100 on a shaker. Alexa Fluor 488–labeled goat anti-rabbit IgG (1:500; Invitrogen, A-11008; RRID: AB_143165) was used as a secondary antibody. Following incubation with a secondary antibody, the brains were washed three times with PBS containing 0.1% Triton X-100 and were mounted using Vectashield (Vector Laboratory, Burlingame, CA). Images were captured on a Leica SP5II confocal microscope (RRID: SCR_018714) with 20-fold magnification. Z-stack images were scanned at 1.5-μm section intervals with a resolution of 512 × 512 pixels. Images were processed with ImageJ (RRID: SCR_018714).

Statistics. The first part of the study was exploratory in nature: accordingly, for electrophysiological recordings, uptake, binding, and cellular pharmacochaperoning studies, the number of independent experiments (n = 3–5) was chosen to verify the reproducibility of the data, and there were not any preplanned statistical tests. Error bars indicate S.D. The appropriate equations for a rectangular hyperbola, monophasic inhibition, monoexponential decay, and monoexponential rise were used for nonlinear least-squares curve fitting to calculate the parameter estimates, which are reported as median values and their 95% confidence intervals (CI). Concentration response curves obtained from electrophysiological recordings were fitted by either shared or separate parameters. An F test was used to verify if a fit with separate parameters gave a statistically significant improvement in the fit. IC_{50} values, which were obtained in binding and uptake assays under two paired conditions (i.e., Na^+- versus K^+-containing buffer, preincubation with inhibitors versus their simultaneous addition with substrate), were compared by a paired t test or a Mann-Whitney rank sum test (if the Shapiro-Wilk test indicated departure from a normal distribution). Multiple statistical comparisons were done by (repeated measures) ANOVA, Kruskal-Wallis, or Friedman test followed by Tukey's, Dunn's, or the Holm-Šidák post hoc test. In this exploratory part, P values are descriptive rather than hypothesis testing. In drosophila experiments, which examined the ability of compounds to restore delivery of SERT-P601A/G602A to the axonal territory, the number of experiments was based a power calculation (>90% probability of finding a statistically significant difference with $P < 0.01$) based on the variation previously observed (Bhat et al., 2023). Comparisons between groups (of differently treated flies) were done by a Kruskal-Wallis test followed by a two-sided Dunn's multiple comparison.

Results

Inhibition of Substrate Uptake through SERT by Vilazodone, Trazodone, and Nefazodone is Insurmountable. Vilazodone was reported to be a noncompetitive inhibitor of SERT (Plenge et al., 2021); consistent with this recent report, we found that increasing concentrations of vilazodone resulted in a progressive reduction in the V_{max} of serotonin uptake (Fig. 1A). However, we observed mixed-competitive inhibition because the K_M of 5-HT rose with increasing concentrations of vilazodone (Table 1). We ascribe this discrepancy to the highly lipophilic nature of vilazodone (Figs. 2 and 8). In contrast and as expected, cocaine resulted in surmountable (i.e.,

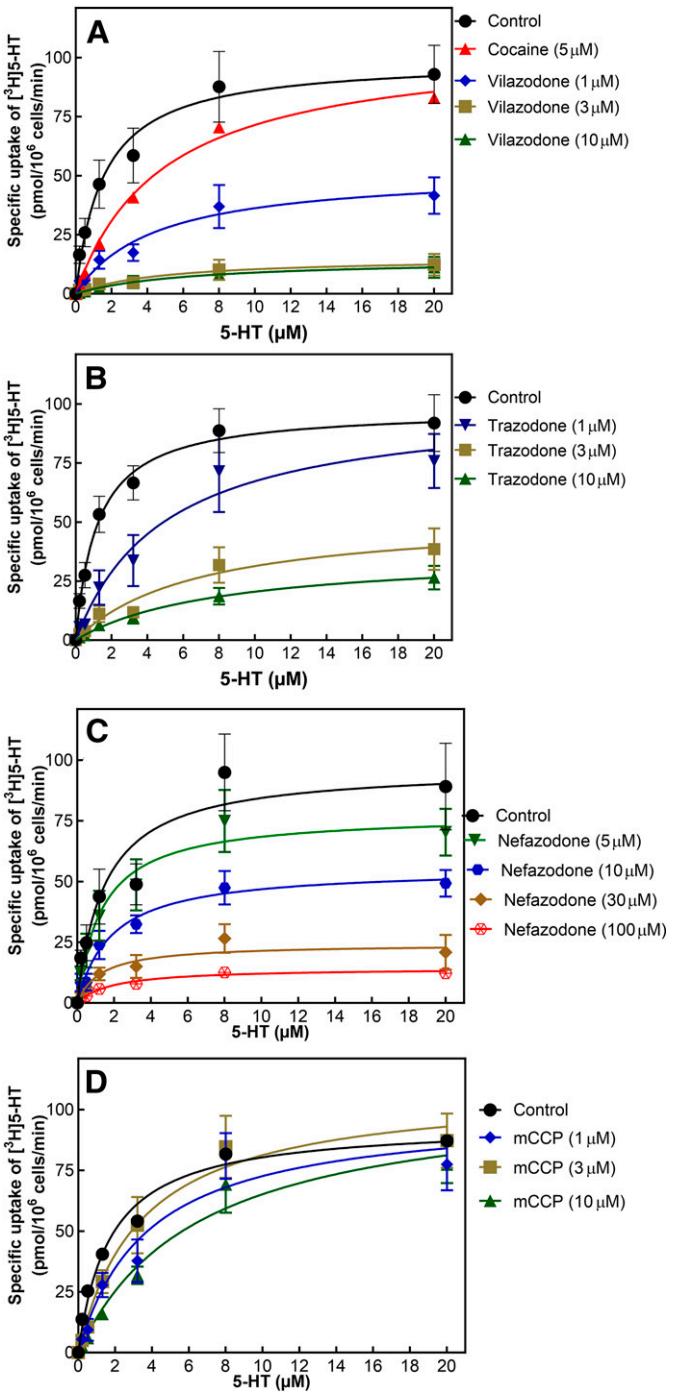

Fig. 1. Inhibition by vilazodone (A), trazodone (B), nefazodone (C), and mCCP (D) of [^{3}H]5-HT uptake by SERT. Substrate uptake by HEK293 cells stably expressing YFP-tagged wild-type SERT was determined as outlined in *Materials and Methods*. The data were obtained from three (A and B) or four (C and D) independent experiments, which were done in triplicates; the error bars indicate S.D. Cocaine (5 μM) was used as an internal control for competitive inhibition in each experiment, but the pertinent data are only shown in (A). Similar, control curves were done in each set of experiments; the displayed control curve is the average from all pooled data (n = 11) and is the same in all panels. The lines were drawn by curve fitting to the equation of a rectangular hyperbola.

competitive) inhibition (red triangles in Fig. 1A; Table 1). Inhibition of substrate uptake by both trazodone (Fig. 1B) and nefazodone (Fig. 1C) was not competitive, i.e., increasing concentrations of these compounds resulted in a progressive

TABLE 1
Effect of vilazodone, trazodone, nefazodone, and mCCP on the kinetics of 5-HT uptake by wild-type SERT
Shown are the median and the 95% confidence intervals. Parameter estimates were obtained by fitting the data shown in Fig. 1 to a rectangular hyperbola. The statistical comparison was done by ANOVA followed by Tukey's post hoc comparison against the K_M and the V_{max} under control conditions; P values are given in parentheses.

	Inhibitor (μM)	V_{max} (pmol min^{-1} 10^{-6} cells)	K_M (μM)
Control (n = 11)	0	99.3 (95.0–103.6)	1.4 (1.2–1.8)
Cocaine (n = 9)	5	106.0 (101.1–111.9) ($P > 0.9999$)	4.9 (4.3–5.5) ($P < 0.0001$)
Vilazodone (n = 3)	1	52.3 (44.2–60.2) ($P < 0.0001$)	3.7 (2.7–6.2) ($P = 0.3186$)
	3	15.3 (11.9–18.7) ($P < 0.0001$)	5.4 (1.9–7.7) ($P = 0.0151$)
	10	14.7 (11.0–18.4) ($P < 0.0001$)	6.1 (2.2–10.6) ($P < 0.0001$)
Trazodone (n = 3)	1	100.8 (85.7–115.8) ($P = 0.9833$)	5.2 (3.2–6.8) ($P = 0.0083$)
	3	52.7 (43.5–61.9) ($P < 0.0001$)	6.4 (3.9–9.8) ($P = 0.0011$)
	10	35.6 (32.0–42.0) ($P < 0.0001$)	8.0 (5.6–10.5) ($P < 0.0001$)
Nefazodone (n = 4)	5	78.4 (71.9–83.6) ($P = 0.002$)	1.4 (1.0–1.7) ($P > 0.9999$)
	10	54.8 (51.5–59.6) ($P < 0.0001$)	2.0 (1.4–2.3) ($P > 0.9999$)
	30	23.6 (21.6–26.9) ($P < 0.0001$)	1.3 (0.8–1.8) ($P > 0.9999$)
	100	14.3 (13.2–15.5) ($P < 0.0001$)	1.9 (1.4–2.4) ($P = 0.9998$)
mCCP (n = 4)	1	99.9 (90.8–108.7) ($P = 0.9993$)	3.3 (2.1–4.4) ($P = 0.1228$)
	3	109.9 (100.4–117.1) ($P = 0.997$)	4.2 (3.1–5.1) ($P = 0.2543$)
	10	107.6 (98.0–117.0) ($P > 0.9999$)	6.2 (5.3–7.9) ($P < 0.0001$)

decline of V_{max}: trazodone gave rise to mixed-competitive inhibition, with the K_M of 5-HT shifting to higher values in the presence of increasing trazodone (Table 1). In contrast, inhibition by nefazodone was noncompetitive because the K_M of 5-HT in the presence of 5, 10, 30, and 100 μM was comparable to that seen in the absence of any inhibitor (Table 1). The metabolite mCPP is a substrate of SERT (Baumann et al., 2014). Accordingly, inhibition of substrate uptake by mCPP was competitive (Fig. 1D): with increasing concentrations of mCPP, the K_M of substrate was shifted to the right, but V_{max} remained constant (Table 1).

We noted that the inhibitory potency of vilazodone was very much dependent on the time when it was added to the uptake assay. This is illustrated by the concentration-response curves shown in Fig. 2A: the IC_{50} of vilazodone was shifted by more than two orders of magnitude to the left if cells were preincubated for 15 minutes with vilazodone, resulting in median IC_{50} values of 6.1 nM (95% CI, 5.7–6.6 nM) and 1.0 μM (95% CI, 0.5–1.9 μM; P = 0.00197, t test for paired values) for 15-minute preincubation and for simultaneous addition, respectively. In contrast, the inhibitory potency of trazodone (Fig. 2B; IC_{50}, 1.8 μM; 95% CI, 1.4–2.1 μM and IC_{50}, 1.6 μM; 95% CI, 1.1–2.4 μM for 15-minute preincubation and for simultaneous addition, respectively; P = 0.897, t test for paired data), of nefazodone (Fig. 2C; IC_{50}, 4.5 μM; 95% CI, 3.0–6.5 μM and 7.5 μM; 95% CI, 6.0–8.4 μM for 15-minute preincubation and for simultaneous addition, respectively; P = 0.063, t test for paired data) and of mCPP (Fig. 2C; IC_{50}, 2.4 μM; 95% CI,

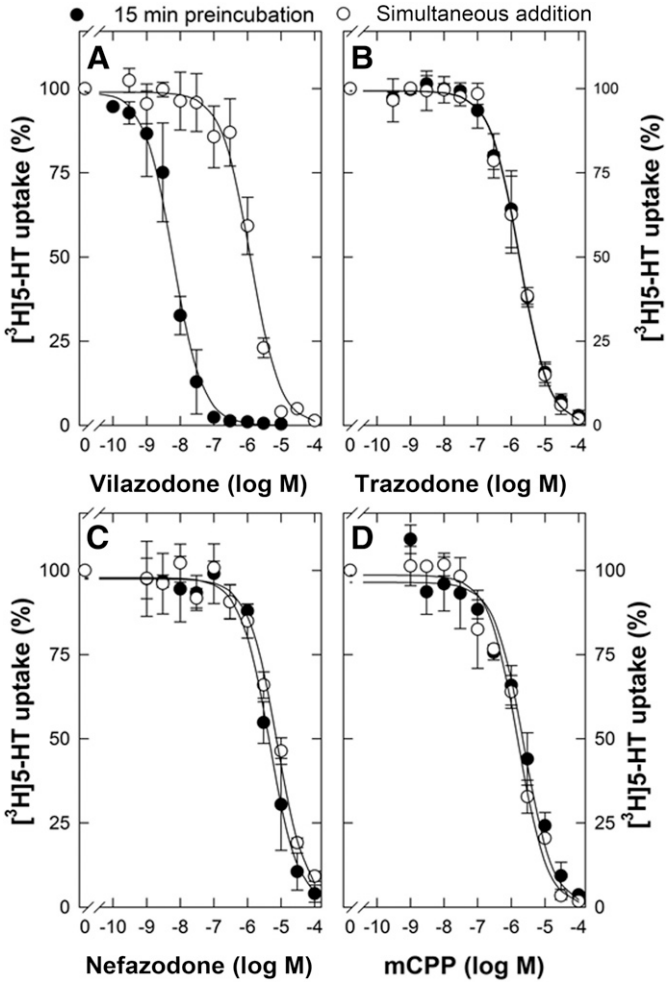

Fig. 2. Concentration-response curves for inhibition of SERT-mediated [^{3}H]5-HT uptake by vilazodone, trazodone, and mCCP. HEK293 cells stably expressing YFP-tagged wild-type SERT were seeded in poly-D-lysine–coated 96-well plates (2×10^5 cells/well). After 24 hours, cells were washed twice with Krebs-HEPES buffer. The uptake reaction was initiated by simultaneous addition (open symbols) of [^{3}H]5-HT (final concentration, 0.1 μM) and the indicated concentrations of vilazodone, trazodone, or mCCP. Alternatively, cells were preincubated for 15 minutes with the indicated concentrations of vilazodone, trazodone, or mCCP, and the uptake reaction was initiated subsequently by the addition of [^{3}H]5-HT (closed symbols). The values of specific uptake in the absence of vilazodone, trazodone, and mCCP were 7.2 ± 0.3, 6.0 ± 0.4, and 6.2 ± 0.6 pmol min^{-1} 10^{-6} cells; these were set to 100% to normalize for interassay variation. Data are means ± S.D. from three independent experiments done in triplicates. The curves were generated by a fit to the equation describing monophasic inhibition.

1.3–3.1 μM and IC_{50}, 1.7 μM; 95% CI, 1.0–2.4 μM for 15-minute preincubation and for simultaneous addition, respectively; $P = 0.256$, t test for paired data) did not depend on the incubation time.

Transport-associated inward currents through SERT can be recorded in the whole-cell patch-clamp configuration if SERT-expressing cells are challenged with substrate. The current has two components: 1) a peak current, which reflects the initial synchronized movement of substrate and cosubstrate through the membrane electric field, and 2) a steady current, which reflects the continuous cycling of the transporter in the forward transport mode (Schicker et al., 2012). Accordingly, we also used electrophysiological recordings to verify that SERT is inhibited by trazodone and nefazodone in a manner that is not competitive: the representative traces in Fig. 3, A and B show that trazodone caused a pronounced inhibition of the steady current. The amplitude of the steady current at saturating 5-HT declined progressively in the presence of increasing trazodone concentrations (Fig. 3C). The same was true for nefazodone (Fig. 3D). We extracted the normalized current amplitudes at a saturating concentration of 5-HT (i.e., 30 μM) from Fig. 3, C and D and plotted them as a function of the trazodone (circles in Fig. 3E) and nefazodone concentration (triangles in Fig. 3E). The IC_{50} values estimated by the fits were 0.37 μM for trazodone and 0.88 μM for nefazodone. We also analyzed the dependence of the substrate K_M on the concentration of the inhibitors. The K_M values were estimated by fitting the saturation curves in Fig. 3, C and D to a rectangular hyperbola. In Fig. 3F, we plotted the K_M of 5-HT as a function of the trazodone and nefazodone concentration. The K_M value of 5-HT increased with the concentration of trazodone. This was not the case for nefazodone. This confirms that trazodone is a mixed-competitive inhibitor of SERT, whereas inhibition by nefazodone is noncompetitive.

Binding of Vilazodone and of Trazodone to SERT Requires the Presence of Sodium. Typical inhibitors such as citalopram, a selective serotonin reuptake inhibitor, bind to the outward-facing state. In the transport cycle of SERT, potassium drives the return step from the inward-facing to the outward-facing conformation (Bhat et al., 2021b). Accordingly, appreciable binding of typical radiolabeled inhibitors can be detected in the presence of potassium, but the binding affinity of these inhibitors and of substrates is substantially higher in the presence of saturating concentrations of sodium than of potassium (Korkhov et al., 2006; Bhat et al., 2023). Atypical inhibitors, which trap SERT in the inward-facing conformation, however, bind either with comparable affinity in the presence of sodium and potassium or bind preferentially in the presence of potassium (Bhat et al., 2023). We therefore examined the ability of vilazodone and trazodone to inhibit binding of [^{3}H]citalopram to SERT in the presence of 120 mM Na^+ versus 120 mM K^+. The ibogaine analog compound 9b (Bhat et al., 2020) was used as internal control (Fig. 4A): as previously shown (Bhat et al., 2023), compound 9b competed with [^{3}H] citalopram binding to SERT with comparable affinity in the presence of 120 mM Na^+ (median IC_{50}, 76 nM; 95% CI, 51–105 nM) and 120 mM K^+ (IC_{50}, 74 nM; 95% CI, 70–79 nM; $P = 0.736$, t test for paired data). In contrast, the inhibition curve for vilazodone (IC_{50}, 5.8 nM; 95% CI, 1.8–10.3 nM and 36.7 nM; 95% CI, 15.5–54.1 nM; $P = 0.00332$, t test for paired data), for trazodone (IC_{50}, 472 nM; 95% CI, 335–624 nM and 4380 nM; 95% CI, 4098–4603 nM; $P = 0.0000000116$, t test for paired data), and for nefazodone (IC_{50}, 747 nM; 95% CI, 610–885 nM and 1490–95% CI, 892–1490 nM; $P = 0.0276$, t test for paired data) was shifted to the right if the binding reaction was conducted in the presence of K^+ (closed and open symbols in Fig. 4, B–D). We note that the shift was most pronounced for trazodone (median, 9.2-fold; 95% CI, 6.6- to 12.0-fold), followed by vilazodone (6.0-fold; 95% CI, 4.7- to 7.0-fold) and nefazodone (2.2-fold; 95% CI, 1.3- to 2.7-fold), with the differences being statistically significant ($P \leq 0.008$; ANOVA followed by all pairwise comparison by the Holm-Šidák test). The metabolite mCPP is a (partial) substrate of SERT (Baumann et al., 2014): as expected for a substrate, the affinity of mCPP for SERT was higher in the presence of Na^+ (median IC_{50}, 608 nM; 95% CI, 584–626 nM) than in the presence of K^+

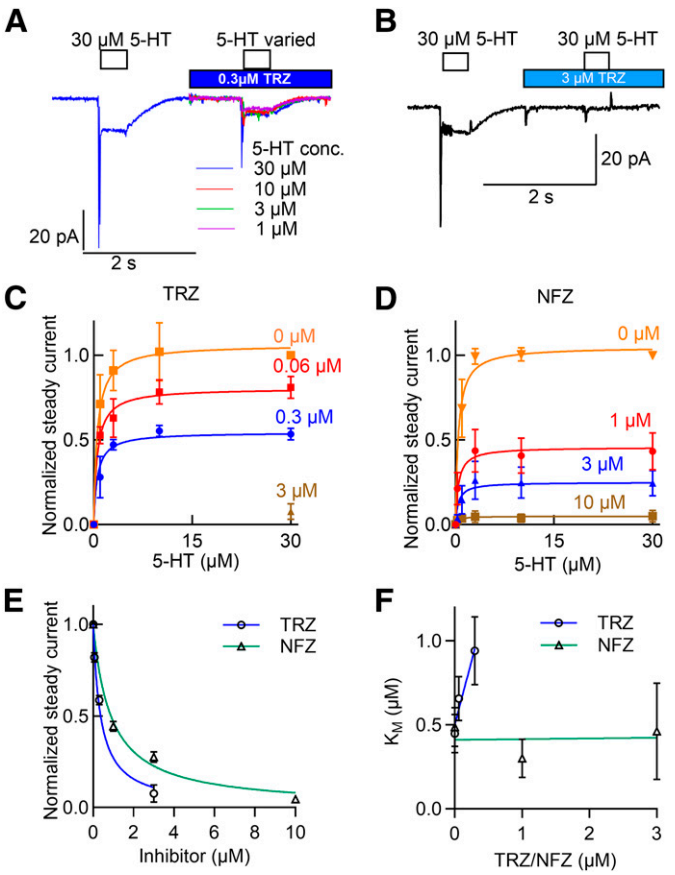

Fig. 3. Mixed-competitive and noncompetitive inhibition by trazodone (TRZ) and nefazodone, respectively, of transport-associated currents through SERT. (A and B) The electrophysiological protocol is illustrated above the representative traces: substrate-induced currents were first evoked by superfusing a HEK293 cell expressing GFP-tagged human SERT in the whole-cell patch-clamp configuration with 30 μM 5-HT (open bar), followed by a washout and a subsequent superfusion with 0.3 (red bar, A) and 3 μM (blue bar, B) trazodone. A second pulse of serotonin at the indicated concentrations was applied in the continuous presence of trazodone. The representative traces show the corresponding currents elicited by the first pulse of 5-HT and the second pulse of increasing 5-HT concentrations in the presence of trazodone. (C and D) The steady current amplitudes were recorded as in (A) and (B), normalized to the amplitude of the first pulse (i.e., 30 μM 5-HT) prior to superfusion with trazodone (C) and nefazodone (NFZ, D) and plotted as a function of the 5-HT concentration. For the control curves (0 μM, orange squares), cells were superfused with buffer. The lines represent the fit to a rectangular hyperbola. V_{max} values differed in a statistically significant manner between curves generated in the absence (control, 0 μM) and presence of trazodone or of nefazodone ($P < 0.001$, F test). (E) The amplitudes of the steady current elicited by 30 μM 5-HT were taken from (C) and (D) and plotted as a function of the trazodone and nefazodone concentration, respectively. The fitted curves gave IC_{50} values of 0.37 μM (95% CI, 0.19–0.71 μM) and 0.88 μM (95% CI, 0.47–1.65 μM) for trazodone (blue) and nefazodone (green), respectively. (F) K_M values were extracted from the curves shown in (C) and (D) and plotted as a function of the trazodone and nefazodone concentration, respectively. The K_M values in the absence and presence of 0.06 and 0.3 μM trazodone were 0.44 μM (95% CI, 0.21–0.68 μM), 0.66 μM (0.39–0.93 μM), and 0.94 μM (0.52 to 1.36 μM), respectively. The K_M values in the absence and presence of 1 and 3 μM nefazodone were 0.45 μM (0.21–0.70 μM), 0.30 (0.065 to 0.54 μM), and 0.46 μM (0.01 to 1.03), respectively. The lines were obtained by linear regression, yielding slopes of 1.52 ± 0.38 (statistically significant correlation, $P = 0.04$) and 0.004 ± 0.066 (no statistically significant correlation, $P = 0.95$) for trazodone (blue) and nefazodone (green), respectively.

(IC_{50}, 3916 nM; 95% CI, 2017–6592 nM; $P = 0.008$, Mann-Whitney rank sum test) (inset to Fig. 4C).

Insurmountable inhibition of substrate uptake is seen if the inhibitor traps the transporter in the inward-facing state

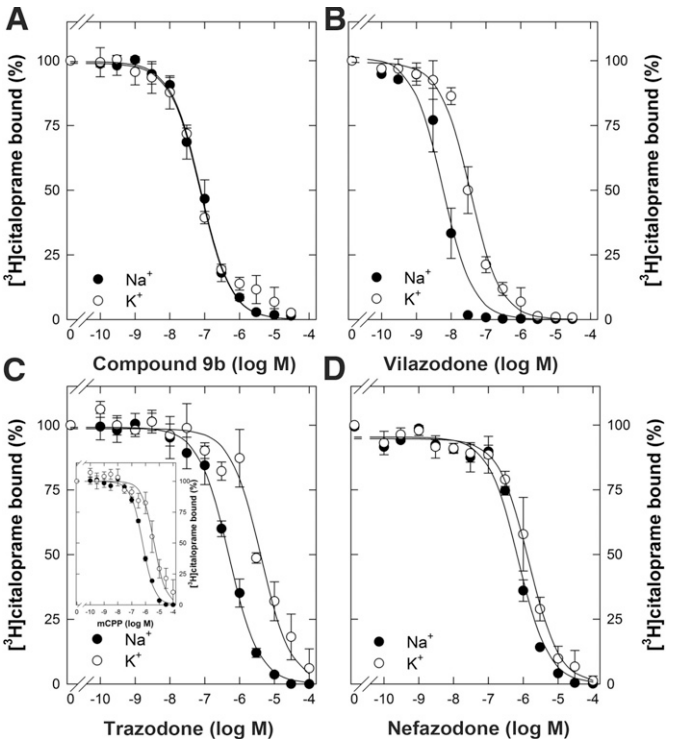

Fig. 4. Inhibition of [^{3}H]citalopram binding to SERT by compound 9b (A), vilazodone (B), trazodone and mCCP (C), and nefazodone (D) in the presence of sodium and potassium. The reactions were done in a binding buffer, which contained either 120 mM Na^+ (closed symbols) or 120 mM K^+ (open symbols) with membranes (about 2.5 μg and 30 μg, respectively) and 3 nM [^{3}H]citalopram. Specific binding in the absence of inhibitor was in the range of 12.5–14.5 pmol mg^{-1} and 0.37–0.45 pmol mg^{-1} for buffer containing 120 mM Na^+ or K^+, respectively, and was set to 100% to normalize for interassay variation. Data are means from three (A, B, and D), five (C), and four (inset to C) independent experiments done in duplicate; error bars represent S.D. The curves were generated by a fit to the equation describing monophasic inhibition.

(Bhat et al., 2023). However, this cannot account for the action of trazodone (and its congeners) because they bound preferentially to the Na^+-promoted, outward-facing state. The alternative possibility is that insurmountable inhibition arises from an allosteric action. In this instance, both substrate and inhibitor can bind simultaneously. Accordingly, we compared the ability of cocaine (Fig. 5A) and of trazodone (Fig. 5C) to inhibit binding of [^{3}H]citalopram to SERT in the presence of serotonin. The data summarized in Fig. 5, A and C were transformed by plotting the reciprocal of bound radioligand as a function of inhibitor concentration to yield Dixon plots (Fig. 5, B and D). Dixon plots allow for differentiating mutually exclusive from mutually nonexclusive binding if one inhibitor (i.e., cocaine or trazodone) is examined at a fixed concentration of the second inhibitor (i.e., serotonin) (Segel, 1975): if the two inhibitors bind to the same site, the slope of the inhibition curves is not affected, resulting in a family of parallel lines. As expected, this was observed for cocaine in the presence of serotonin (Fig. 5B). In contrast, a family of lines of progressively increasing slope is seen if binding of the two inhibitors is mutually nonexclusive. This was seen for trazodone (Fig. 5D). Thus, binding of serotonin and of trazodone to SERT occurred concomitantly and to different sites.

Determination by Electrophysiological Recordings of the Binding Kinetics of Trazodone and Vilazodone. The experiments summarized in Fig. 4 indicate that trazodone

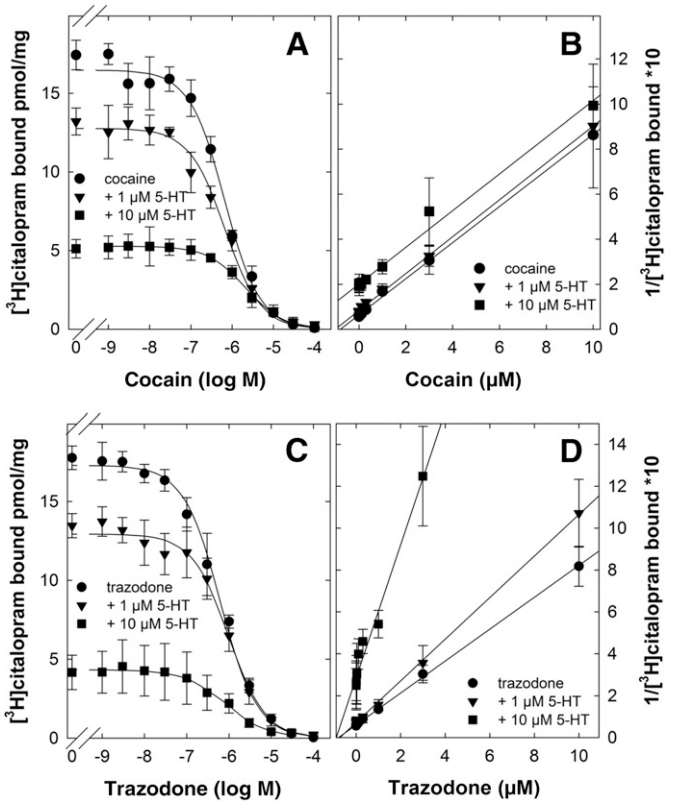

Fig. 5. Inhibition of [^{3}H]citalopram binding to SERT by cocaine (A) and trazodone (C) in the absence and presence of serotonin. The reactions were done in a binding buffer, which contained 120 mM Na^+ with membranes (about 3 µg) and 4 nM [^{3}H]citalopram in the absence (circles) and presence of 1 (triangles) and 10 µM serotonin (squares). Data are means from three independent experiments done in duplicate; error bars represent S.D. The curves were generated by a fit to the equation describing monophasic inhibition. (B) and (D) show the transformation of the data of (A) and (C), respectively, into Dixon plots.

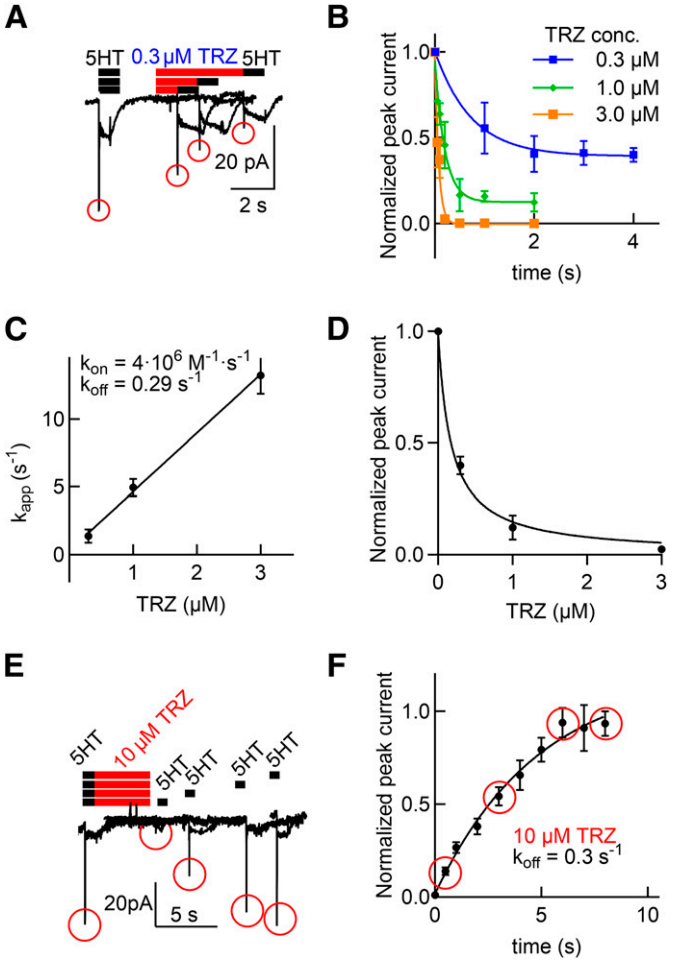

Fig. 6. Kinetics of trazodone (TRZ) binding to SERT. (A) The protocol used to assess the association kinetics of trazodone is illustrated above the representative traces: substrate-induced currents were evoked by superfusing a HEK293 cell expressing GFP-tagged human SERT in the whole-cell patch-clamp configuration with 30 µM 5-HT (black bar) before and after application of 0.3 µM trazodone for a period of 1, 2, and 4 seconds (red bar). (B) The resulting ratios of 5-HT–induced peak current amplitudes before and after the application of trazodone were plotted as a function of the exposure time to the indicated concentrations of trazodone. Data are means ± S.D. from 5–9 independent recordings. The lines were drawn by fitting the data to a monoexponential function. Separate fitting to three curves was significantly better than to a single curve with shared parameters ($P = 0.0001$, F test). Accordingly, both the extent of steady current inhibition and the k_{app} values depended on the trazodone concentration. (C) The extracted k_{app} values were plotted as a function of trazodone concentration; error bars indicate S.D. The k_{on} ($4.3{\cdot}10^6$ $M^{-1}{\cdot}s^{-1}$) and k_{off} values (0.29 $seconds^{-1}$) were obtained from the y-intercept and the slope of the regression line, respectively. (D) The inhibition of the peak current amplitude at steady-state was plotted as a function of the trazodone concentration to calculate an IC_{50} of 173 nM (95% CI, 145–201 nM). (E) The protocol used to assess the dissociation kinetics of trazodone is illustrated above the representative traces: substrate-induced currents were evoked by superfusing a HEK293 cell expressing GFP-tagged human SERT in the whole-cell patch-clamp configuration with 30 µM 5-HT (black bars) before application of 10 µM trazodone (red bar) for a period of 7 seconds (red bar). The subsequent washout period was varied in length prior to reapplication of the second 5-HT pulse. The representative traces show that the peak current recovered over time. (F) The peak current amplitude elicited by the second pulse of 5-HT was compared with the peak current amplitude of the control 5-HT pulse, and the ratios were plotted as a function of the length of the washout period. A monoexponential fit yielded a k_{off} of 0.30 $seconds^{-1}$ (95% CI, 0.25–0.36 $seconds^{-1}$). Data are means ± S.D. from 5–9 independent recordings. k_{app}, apparent rate of association.

and its congeners (vilazodone and nefazodone) gain access to their binding site(s) in the Na^+-promoted, outward-facing conformation. The on and off rate for binding of inhibitors to the outward-facing state can be assessed by monitoring their time-dependent effect on the substrate-evoked peak current through SERT (Hasenhuetl et al., 2015). Accordingly, we first recorded the substrate-induced current prior to and after superfusion of HEK293 cells stably expressing GFP-tagged SERT with trazodone for variable time intervals to obtain the association rate constant: the amplitude of the peak current declined as the time interval of trazodone exposure was increased (Fig. 6A). This approach allowed for assessing the time course of the trazodone-induced inhibition by comparing the peak current amplitude evoked by 5-HT prior to and after application of trazodone as a function of time. It is evident from Fig. 6B that 1) raising the concentration of trazodone accelerated the onset of inhibition and that 2) the time course of inhibition was adequately described by a monoexponential decay. We extracted the apparent rates and plotted these k_{app} values as a function of trazodone concentration (Fig. 6C): the slope and the y-intercept allowed for estimating the association rate constant (k_{on}) and the dissociation rate constant (k_{off}), respectively. A kinetic K_D of 72.5 nM was estimated from the ratio k_{off}/k_{on}. This is in reasonable agreement with the

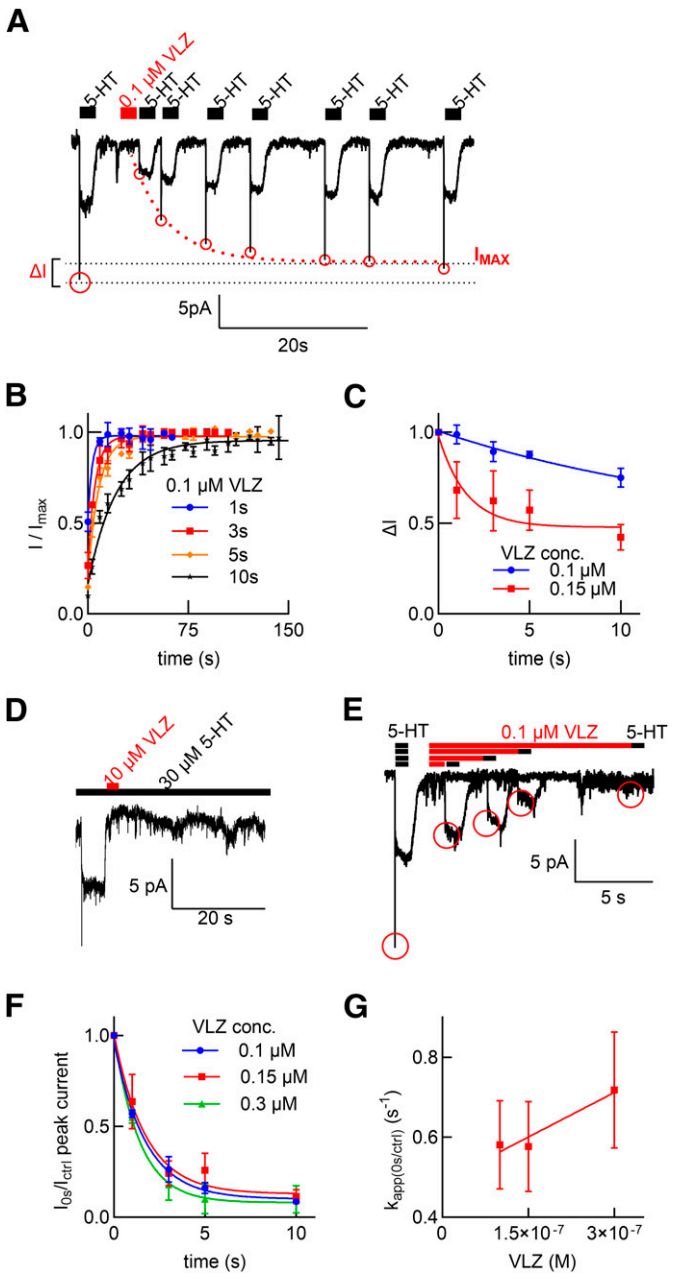

Fig. 7. Kinetics of vilazodone (VLZ) binding to SERT. (A) Vilazodone dissociation kinetics were determined with the protocol illustrated above the representative traces: substrate-induced currents were evoked by superfusing a HEK293 cell expressing GFP-tagged human SERT in the whole-cell patch-clamp configuration with 30 μM 5-HT (white bar). After washout, the cell was superfused with 100 nM vilazodone (red bar) for 3 seconds followed by 5-HT pulses (white boxes) at the indicated intervals. The representative traces show the time course of peak current recovery, which reflects the rate of vilazodone dissociation. The amplitude of the current did not recover to the amplitude elicited by the initial control pulse: the lost fraction of the current ΔI is indicated by the dashed lines. (B) The time course of peak current recovery was measured as in (A) after increasing time intervals (1, 3, 5, and 10 seconds) of exposure to 100 nM vilazodone. The current amplitudes were normalized to I_{max}, the amplitude reached at steady state, and plotted as a function of the length of the washout period: the time course of peak current recovery depended on the length of exposure to vilazodone, namely yielding estimates of k_{off} = 0.31 seconds^{-1} (95% CI, 0.20–0.42 seconds^{-1}), 0.18 seconds^{-1} (95% CI, 0.14–0.22 seconds^{-1}), 0.12 seconds^{-1} (95% CI, 0.10–0.14 seconds^{-1}), and 0.047 seconds^{-1} (95% CI, 0.041–0.0547 seconds^{-1}) for 1-, 3-, 5-, and 10-second exposure, respectively. (C) ΔI was plotted as a function of the exposure time to 100 nM and 150 nM vilazodone to highlight that ΔI increased with both the exposure time to and the concentration of vilazodone. (D) Quasi-irreversible inhibition of SERT by vilazodone: the representative trace illustrates that, in the continuous presence of 30 μM 5-HT (black bar), superfusion with 10 μM vilazodone for 2 seconds (red bar) fully suppressed the substrate-induced steady current, which did not recover over the next >30 seconds in spite of the removal of vilazodone. (E) Representative currents elicited by the protocol (illustrated above the traces) employed to measure the association rate of vilazodone: vilazodone (100 nM) was applied for variable intervals (red bars) followed immediately by superfusion with 30 μM 5-HT (black bars). (F) The ratio of 5-HT–induced peak current elicited by 5-HT before and after vilazodone was plotted as a function of the time of vilazodone exposure. The lines represent the fit to a monoexponential decay. (G) The apparent rates of association (k_{app}) were extracted from the fit in (F) and plotted as a function of the vilazodone concentration. The values for k_{on} = 0.7·10^6 M^{-1} s^{-1} and k_{off} = 0.6 seconds^{-1} of vilazodone were determined from the slope and the y-intercept of the regression line, respectively.

IC_{50} value (0.23 μM) estimated from the steady-state inhibition of the peak current (Fig. 6D).

We independently estimated the dissociation rate constant of trazodone by measuring recovery of the peak current from inactivation. The protocol required for this approach is illustrated in Fig. 6E: after the substrate-evoked current was measured, the cells were superfused for a defined time interval (7 seconds) with 10 μM trazodone and challenged again with 30 μM 5-HT after increasing intervals of washout. It is evident from the representative traces shown in Fig. 6E that the amplitude of the peak progressively recovered as the intervening washout phase was increased. Peak current recovery, which reflects the time-dependent unbinding of trazodone, was adequately described by a monoexponential rise. An estimate of 0.3 seconds^{-1} was extracted for the k_{off} (Fig. 6F), which is in excellent agreement with the k_{off} estimate obtained from the y-intercept in Fig. 6C.

The approach outlined in Fig. 6 was also used to examine the kinetics of vilazodone binding to SERT. We first attempted to determine the dissociation rate of vilazodone by recording the recovery of the peak current from inactivation: if HEK293 cells stably expressing GFP-tagged SERT were exposed for 3 seconds to 100 nM vilazodone, the peak current recovered rapidly (τ = 0.19 seconds^{-1}; traces in Fig. 7A, red squares in Fig. 7B). However, the peak current did not fully recover (the difference between the current amplitude elicited by the initial pulse of 5-HT and the amplitude reached after steady state of recovery is illustrated as ΔI in Fig. 7A). It is worth pointing out that cells were exposed to trazodone for 7 seconds in Fig. 6, which allowed for full recovery of the peak current amplitude. In addition, the time course of recovery was progressively delayed as the incubation time with 100 nM vilazodone was prolonged (Fig. 7B). This was also true for the loss in peak current amplitude ΔI, which increased with both incubation time and vilazodone concentration (Fig. 7C). This suggested that a fraction of SERT was inhibited by vilazodone in a quasi-irreversible manner. This is also evident from Fig. 7D: if the steady-state current through SERT was evoked by superfusing cells with 30 μM 5-HT, the current was completely suppressed by brief (i.e., 2 seconds) exposure to 10 μM vilazodone. Importantly, the current did not recover to any appreciable extent, although SERT were continuously superfused with 5-HT for more than 30 seconds.

The rate of vilazodone binding was estimated by recording the decline in peak current amplitude arising from superfusing cells with 100, 150, and 300 nM vilazodone for increasing time

intervals (Fig. 7, E and F). It is evident that the time course of inhibition by 300 nM vilazodone (green triangles in Fig. 7F) was slower than that resulting from 300 nM trazodone (blue squares in Fig. 6B). The quasi-irreversible component exerted by vilazodone compounded the analysis and precluded the use of higher concentrations. Nevertheless, the initial binding event, which drives the interaction of vilazodone with SERT, is not of high affinity: it is evident from the time course of peak current recovery after exposure to 100 nM vilazodone (Fig. 7, A and B) that vilazodone unbinds rapidly provided that the exposure time is short. The recovery curve with the shortest exposure time (1 second, blue squares in Fig. 7B) allows for estimating k_{off} in the range of 0.3 seconds^{-1}. However, it is obvious from the data shown in Fig. 7B that this k_{off} is an underestimate of the true k_{off}. The k_{off} estimated from the y-intercept in Fig. 7G is 0.6 seconds^{-1}, but there is

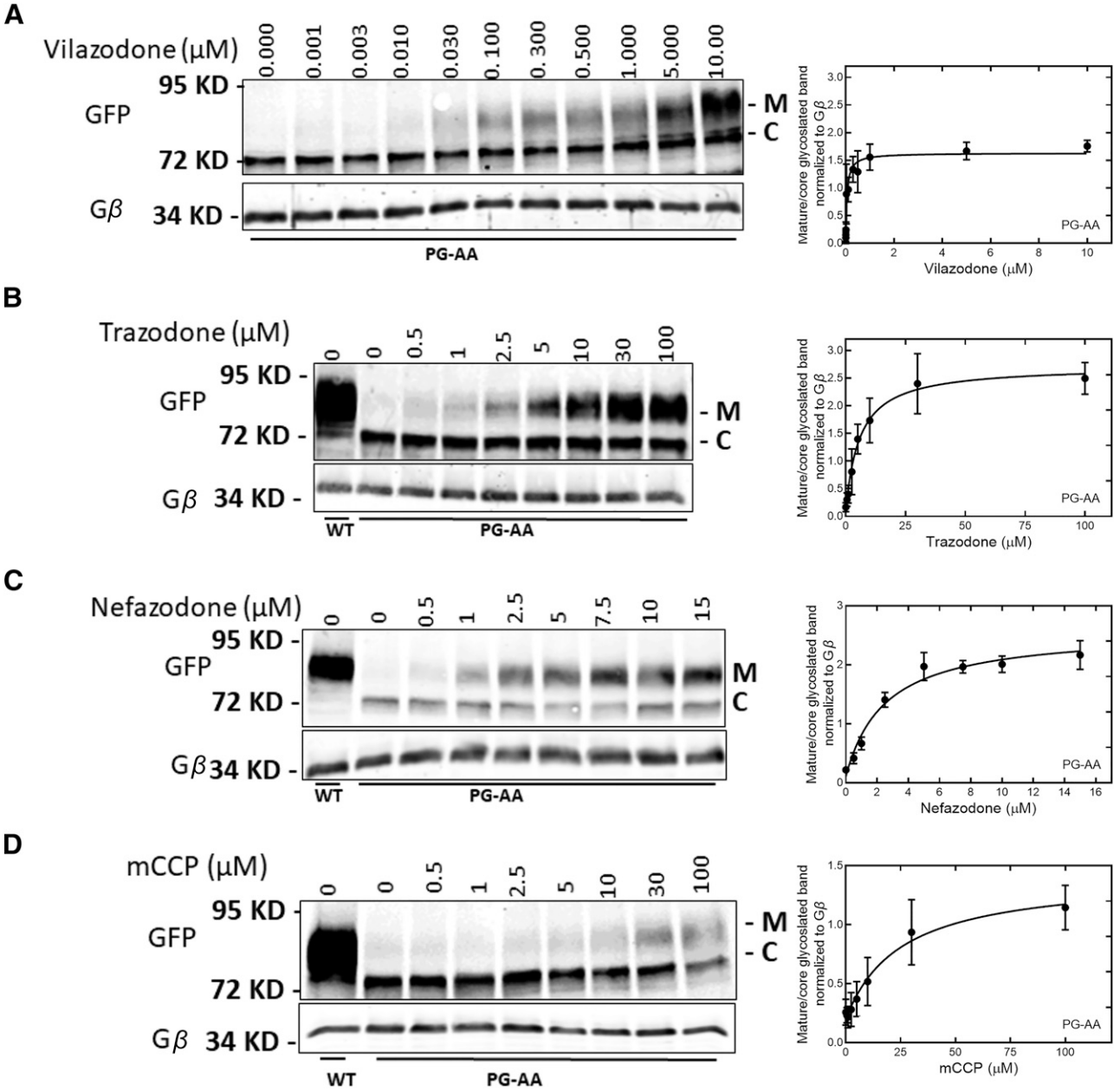

Fig. 8. Vilazodone (A), trazodone (B), nefazodone (C), and mCCP (D) rescue folding-deficient SERT-P601A/G602A. Cell lysates were prepared from HEK293 cells stably expressing YFP-tagged wild-type SERT (WT) or from HEK293 expressing SERT-P601A/G602A (PG-AA), which had been incubated with the indicated concentrations of vilazodone (A), trazodone (B), nefazodone (C), and mCCP (D). Aliquots of detergent lysates (30 μg) were electrophoretically resolved and transferred onto nitrocellulose membranes. The immunoreactivity was detected with antibodies directed against anti-GFP antibody and G protein β-subunits (Gβ) to visualize YFP-tagged SERT and the loading control Gβ, respectively. The blots shown in (A–C) are representative of three (A–C) and five (D) independent experiments. The immunoreactive bands in panels were quantified using imageJ to calculate the ratio of mature (M) to ER-resident, core-glycosylated band (C). This ratio [means ± S.D.; $n = 3$ in (A–C) and $n = 5$ in (D)] was plotted as a function of ligand concentration on the right-hand side. The curves were drawn by fitting the equation for a rectangular hyperbola to the data points. A statistical comparison of the control value (i.e., the ratio of mature to core glycosylated band in the absence of cellular preincubation with any compound) to the values obtained in the presence of compounds was done by repeated measures ANOVA followed by the Holm-Šidák post hoc test: this showed a significant effect ($P \leq 0.01$) for vilazodone (A), trazodone (B), nefazodone (C), and m-CPP (D) at concentrations ≥0.03, 2.5, 1, and 10 μM, respectively.

a large error associated with this estimate. In spite of these caveats, the K_D calculated from the ratio of k_{off}/k_{on} is in the range of 0.4–0.9 μM and thus in the range of the IC_{50}, which was observed if inhibition of substrate was assessed without preincubation (*cf*. Fig. 2A).

Trazodone and Its Congeners Are Effective Pharmacochaperones. Taken together, the observations suggested that the binding mode of trazodone, nefazodone, and vilazodone differed substantially from typical inhibitors. Because of this atypical binding mode, we explored the conjecture that these compounds also acted as pharmacochaperones. Accordingly, we incubated cells expressing YFP-tagged SERT-P601A/G602A for 24 hours in the presence of increasing concentrations of these compounds. SERT-P601A/G602A is a severely misfolded mutant, which is retained in the endoplasmic reticulum but is amenable to rescue by noribogaine (El-Kasaby et al., 2014), its congeners (Bhat et al., 2020), other atypical inhibitors (Bhat et al., 2023), and partial substrates (Bhat et al., 2017). As anticipated from its folding deficiency, in the absence of pharmacochaperones, SERT-P601A/G602A accumulated exclusively as ER-resident core-glycosylated species (band labeled C in Fig. 8, A–D). Incubation with vilazodone (Fig. 8A), trazodone (Fig. 8B), nefazodone (Fig. 8C), and mCPP (Fig. 8D) led to a concentration-dependent appearance of a species, which carried mature glycans (band labeled M in Fig. 8, A–D) and thus migrated with slower mobility. This upper band comigrated with the predominant band of wild-type SERT (left-hand lanes in Fig. 8, B–D). We quantified the ratio of upper and lower band to generate concentration response curves (right-hand graphs in Fig. 8, A–D). A rectangular hyperbola was fitted to the data points. The estimated values for the EC_{50} of the pharmacochaperoning effect of the compounds is shown in Table 2 (left-hand column).

SERT is subject to constitutive clathrin-dependent endocytosis (Koban and Freissmuth, 2023). It is conceivable that a fraction of SERT-P601A/G602A escapes from the ER to the cell surface but is rapidly cleared by endocytosis. In this alternative scenario, the action of trazodone and its congeners does not arise from pharmacochaperoning in the ER but from blockage of SERT internalization at the cell surface. We examined this scenario by imposing a cycloheximide block to translation for 2 or 4 hours (Kusek et al., 2015), either after an incubation for 4 hours in the absence and presence of vilazodone, trazodone, or nefazodone (Fig. 9, A and B) or prior to this incubation (Fig. 9, C and D). It is evident that ER export (i.e., appearance of the mature band) was also observed if the cycloheximide-induced block was imposed 4 hours prior to the addition of vilazodone, trazodone, or nefazodone to the cells (Fig. 9, C and D). Thus, the action of these compounds is accounted for by a pharmacochaperoning effect on the ER resident SERT-P601A/G602A rather than a hypothetical inhibition of transporter internalization. We also explored whether these three compounds affected ER export of wild-type SERT. This was not the case: incubation of cells in the presence of vilazodone, trazodone, or nefazodone did not affect the level of the mature band (Fig. 9, E and F).

We verified that the preincubation with the compounds did not only restore ER export but also delivery of functionally active SERT-P601A/G602A to the cell surface by measuring cellular uptake of substrate (Fig. 10). It was not possible to remove vilazodone by washing cells with buffer. This is illustrated with the control incubation of HEK293 cells harboring wild-type SERT (black circles in Fig. 10A). Various regimens were tried, including acid washes (Bhat et al., 2017) and incubation with lipid emulsions (Intralipid) (Ok et al., 2018). These were ineffective (data not shown). The only approach that allowed for partial reversal of the persistent vilazodone-induced inhibition was repeated washing of cells with milk (red squares in Fig. 10A). Under these conditions, it was evident that preincubation with vilazodone partially rescued SERT-P601A/G602A: consistent with the data shown in Fig. 8A, transport activity was restored in cells exposed to concentrations of vilazodone in the nM range (brown triangles in Fig. 10A). However, the full extent of the pharmacochaperoning action of vilazodone was still masked by the residual inhibition. Hence, it was not possible to estimate an EC_{50} for vilazodone.

The rapid dissociation kinetics (*cf*. Fig. 6) predicted that trazodone was readily removed after the preincubation. This was the case. Preincubation with trazodone rescued the folding deficiency and restored substrate transport by SERT-P601A/G602A (Fig. 10B). In fact, the estimated EC_{50} for promoting 5-HT uptake was comparable to the EC_{50} estimated for restoring ER export (Table 2). Nefazodone was the most efficacious pharmacochaperone (Fig. 10C), and the EC_{50} was again in excellent agreement to that estimated for restoring ER export (Table 2). Similarly, and consistent with the data shown in Fig. 10D, mCPP was a less potent (Table 2) and less efficacious pharmacochaperone than trazodone (*cf*. maximum effect E_{max} in Figs. 9B and 10C).

Nefazodone, Trazodone, and Vilazodone Restore Presynaptic Expression of Folding-Deficient hSERT-PG 601 and 602 AA in the Adult Fly Brain. We examined if trazodone and its congeners exert pharmacochaperoning effect in vivo using *Drosophila* as a model organism. Earlier studies using humanized flies expressing human SERT and DAT have shown that the folding-deficient transporters are amenable to pharmacochaperoning (Kasture et al., 2016; Asjad et al., 2017; Bhat et al., 2020, 2023). The adult fly brain contains 80 serotonergic neurons (Kasture et al., 2018). The TRH-T2A-Gal4 driver line was used to drive the expression membrane–bound GFP (mCD8-GFP) in serotonergic neurons to visualize their somata and their axonal projections: it is evident that these serotonergic projections are widely distributed (Fig. 11, C and Cii). We focused on the FB6K-type serotonergic neurons: there are two of these per hemisphere, but their cell bodies are stacked over each other and thus—at the

TABLE 2

EC_{50} values of vilazodone, trazodone, nefazodone, and mCCP in restoring ER export (assessed by immunoblotting) of and 5-HT uptake by SERT-P601A/G602A

Shown are the median and the 95% confidence intervals. Parameter estimates were obtained by fitting the data shown in Fig. 8 (left hand column) and Fig. 10 (right hand column) to a rectangular hyperbola.

	Immunoblotting EC_{50} (μM)	Substrate Uptake EC_{50} (μM)
Vilazodone	0.057 (0.017–0.097) (n = 3)	n.d.
Trazodone	5.8 (2.5–9.2) (n = 3)	3.9 (2.0–5.7) (n = 3)
Nefazodone	2.5 (1.3–3.8) (n = 3)	2.4 (1.2–3.7) (n = 4)
mCCP	24.9 (6.2–43.6) (n = 5)	15.3 (1.9–28.8) (n = 3)

N.d., not determined, because of resistance of vilazodone to washout.

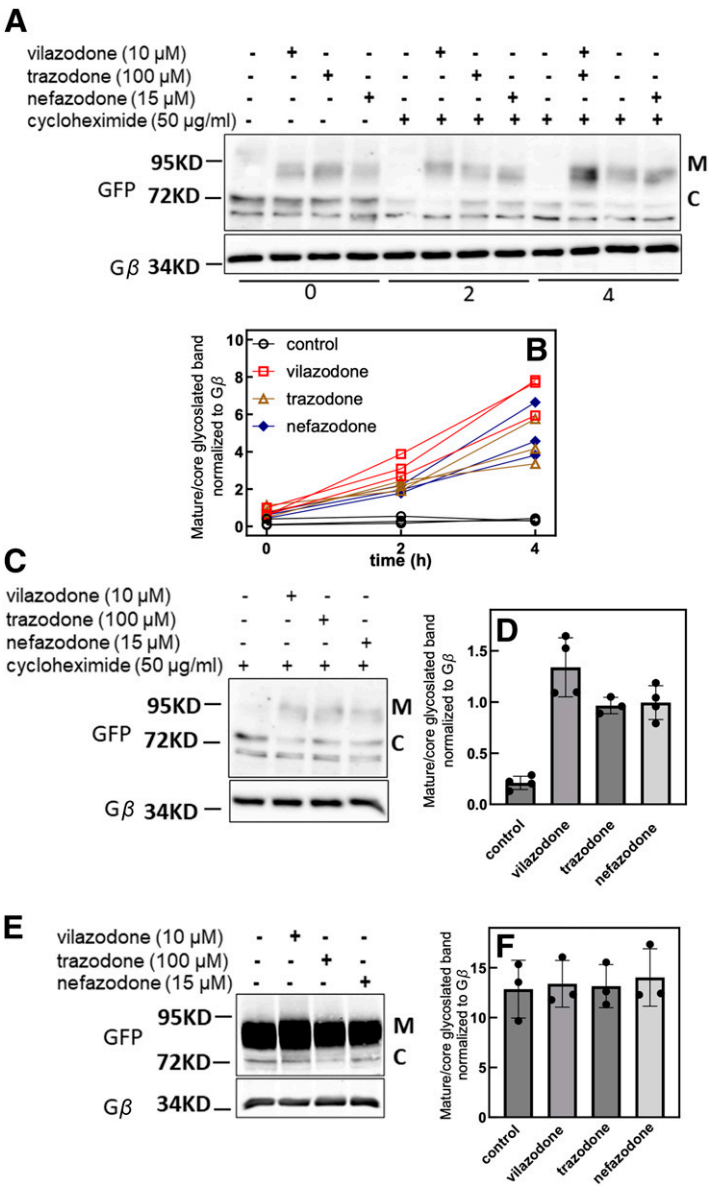

Fig. 9. Folding-deficient SERT-P601A/G602A is rescued during (A and B) and after (C and D) a cycloheximide (CHX) block, but vilazodone, trazodone, and nefazodone do not enhance ER export of wild-type SERT (WT) (E). (A and B) HEK293 cells stably expressing YFP-tagged SERT-P601A/G602A (PG-AA) were preincubated for 4 hours in the absence (control) and presence of vilazodone (10 μM), trazodone (100 μM), or nefazodone (15 μM). Thereafter (time = 0), cycloheximide (50 μg/ml) was added to the cells, which were then incubated for a further 2 or 4 hours. YFP-tagged SERT and Gβ were visualized by immunoblotting, and the quantification was done as in Fig. 8. The blot (A) is representative of three independent experiments, the quantification of which is shown in (B): the lines connect data point from individual experiments. Two-way repeated measures ANOVA (factor time and treatment) showed that there was a statistically significant increase over time ($P < 0.05$) in the ratio of mature over core-glycosylated band (M/C ratio) in the presence all three compounds versus the corresponding control M/C ratio. (C and D) The cells were first incubated with cycloheximide for 2 hours followed by another 4 hours in the absence and presence of vilazodone, trazodone, or nefazodone. Subsequently, cellular lysates were prepared and the proteins were electrophoretically resolved and detected by blotting as described above. The blot (C) is representative of four independent experiments, the quantification of which is shown in (D): results from individual experiments are shown as dots; bars represent the means ± S.D. There was a significant difference ($P < 0.05$, Friedman-test followed by Dunn's post hoc test) between the M/C ratio in the absence and presence of the compounds. (E and F) Cell lysates were prepared from HEK293 cells stably expressing YFP-tagged wild-type SERT, which had been incubated in the absence (control) and presence of (10 μM), trazodone (100 μM), or nefazodone (15 μM) for 24 hours. The bar diagram shows the means ± S.D from three independent experiments. Dots indicate the results from these individual experiments.

resolution shown in the images of Fig. 11—usually coalesce into a single fluorescent soma (white arrows in Fig. 11) The FB6K neurons innervate the presynaptic neuropil of the dorsal fan-shaped body (FB) (Fig. 11, A, C, and Cii). Similar to mCD8-GFP, YFP-tagged wild-type SERT was also visualized in both the FB6K somata and presynaptic FB neuropil and many other areas of the fly brain (Fig. 11, D' and D). The distribution of YFP-tagged wild-type SERT did not change if flies that expressed YFP-tagged wild-type SERT were administered trazodone via their food (Fig. 11, E and Eii). In contrast, SERT-P601A/G602A only accumulated at the site of its synthesis in the cell bodies of FB6K-type neurons (Fig. 11Fii) and was not delivered to the FB neuropil or the other axonal territories of the fly brain (Fig. 11F). This SERT-P601A/G602A pattern was also seen in flies, that had been administered DMSO (vehicle)-containing food (Fig. 11, G and Gii). However, SERT-P601A/G602A reached the presynaptic FB neuropil and the other axonal territories if flies were fed food pellets containing trazodone (Fig. 11, H and Hii), vilazodone (Fig. 11, I and Iii), and nefazodone (Fig. 11, J and Jii). The fluorescence signal in the dorsal FB neuropil was quantified by Imaris 9.3 (Bitplane) in >10 flies/condition to verify that the pharmacochaperoning effect was consistently observed (Fig. 11B).

Discussion

Folding diseases arise from point mutations, which impair the ability of a protein to reach its native conformation. With a few notable exceptions, which are prevalent in certain populations (e.g., sickle cell anemia), individual folding diseases are rare, but collectively they account for a large proportion of hereditary diseases: based on systematic sampling, a substantial fraction (about 28%) of the more than 100,000 identified disease-associated coding variants can be inferred to affect folding of the encoded protein (Sahni et al., 2015). In

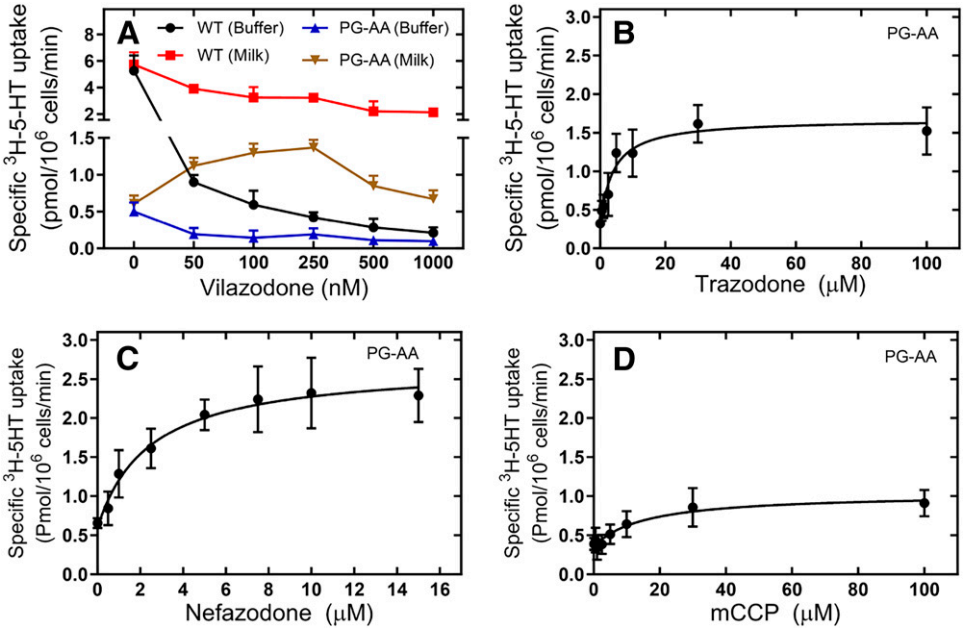

Fig. 10. Preincubation of HEK293 cells expressing folding-deficient SERT-P601/A-G602A with vilazodone, trazodone, nefazodone, and mCCP restores [^{3}H]5-HT uptake. HEK293 stably expressing YFP-tagged SERT-P601A/G602A (PG-AA) were preincubated with the indicated concentrations of vilazodone (A), trazodone (B), nefazodone (C), and mCCP (D) for 24 hours. As a control, HEK293 cells expressing stably expressing wild-type SERT (WT) were also preincubated with vilazodone. Subsequently, the medium was removed; cells preincubated with vilazodone were washed either with Krebs-HEPES buffer (buffer) or with milk; cells preincubated with trazodone and mCPP were washed with Krebs-HEPES buffer, and uptake of 0.1 μM [3H]5-HT was subsequently determined as described in *Material and Methods*. Data are means ± S.D. from three (A–C) and four (D) independent experiments done in triplicate. The curves in (B–D) were drawn by fitting a rectangular hyperbola. A statistical comparison of the control value (i.e., substrate uptake in the absence of cellular preincubation with any compound) to the values obtained after preincubation with compounds was done by repeated measures ANOVA followed by the Holm-Šidák post hoc test: this showed a significant effect ($P \leq 0.04$) for trazodone, nefazodone, and m-CPP at concentrations ≥1, 0.5, and 30 μM, respectively). Similarly, there was a significant difference ($P \leq 0.03$, t test for paired data) in substrate uptake by cells subjected to washes with PBS and with milk following preincubation with vilazodone.

the past 2 decades, the list of disease-associated coding variants in SLC family members has been rapidly expanding (Bhat et al., 2021a). In the SLC6 family, the vast majority of point mutations result in a folding defect (Freissmuth et al., 2018; Bhat et al., 2021a). Misfolding can be corrected by chemical and pharmacological chaperones. Pharmacochaperones bind to and stabilize unfolded or partially folded intermediates. They also shift the folding equilibrium to the fully folded native state and prevent backward reaction while reducing energy barriers during the folding trajectory (Marinko et al., 2019). The rich pharmacology of the monoamine transporters SERT, DAT, and NET provides a treasure trove in the search for pharmacochaperones: typical inhibitors (e.g., tricyclic antidepressants, selective serotonin reuptake inhibitors, selective noradrenaline reuptake inhibitors, cocaine, methylphenidate, etc.), which bind to the orthosteric site and stabilize the outward-facing conformation, are ineffective (Bhat et al., 2019). All pharmacochaperones that have been identified up to now are atypical orthosteric ligands. They bind to and stabilize the inward-facing conformation (El-Kasaby et al., 2010, 2014; Beerepoot et al., 2016; Kasture et al., 2016; Asjad et al., 2017; Bhat et al., 2017, 2020, 2023; Sutton et al., 2022). Here, we examined the actions of the antidepressants trazodone, nefazodone, and vilazodone. Two independent approaches (i.e., substrate uptake assays and electrophysiological recordings) showed that their action did not conform to competitive inhibition. Vilazodone was visualized in the allosteric S2 site of SERT by cryo-electron microscopy (Plenge et al., 2021). In addition, the experiments summarized in Fig. 5 show that trazodone and serotonin can bind simultaneously to SERT. Hence, it is reasonable to posit that, based on their structural similarity, trazodone and nefazodone can also occupy the S2 site and that this underlies their allosteric action. In intact cells, vilazodone stabilizes SERT in the outward-facing conformation (Li et al., 2022). We also found that, unlike the noribogaine analog compound 9b (Bhat et al., 2020), trazodone, nefazodone, and vilazodone preferred the Na^+-bound, outward-facing conformation. In spite of this conformational preference, trazodone, nefazodone, and vilazodone are effective pharmacochaperones: they rescue the severely misfolded variant SERT-P601A/G602A. This conclusion is based on three independent lines of evidence, i.e., 1) restoration of ER-export and 2) of substrate translocation in transfected cells and of 3) delivery to the axonal territory in transgenic flies. Thus, taken together, the current observations provide formal proof for the conclusion that pharmacochaperoning of SERT and, by inference, of other related transporters can be achieved by allosteric ligands.

The folding trajectory of membrane proteins remains elusive (Marinko et al., 2019). Several arguments support the assumption that, in SERT and other SLC6 transporters, the folding trajectory moves through the inward-facing conformation (Freissmuth et al., 2018): 1) the ionic conditions in the endoplasmic reticulum favor the inward-facing conformation; 2) a mutation, which traps SERT in the inward-facing conformation, acts as second-site suppressors: it restores ER export and cell surface delivery of several folding-deficient variants of SERT (Koban et al., 2015); and 3) orthosteric ligands only

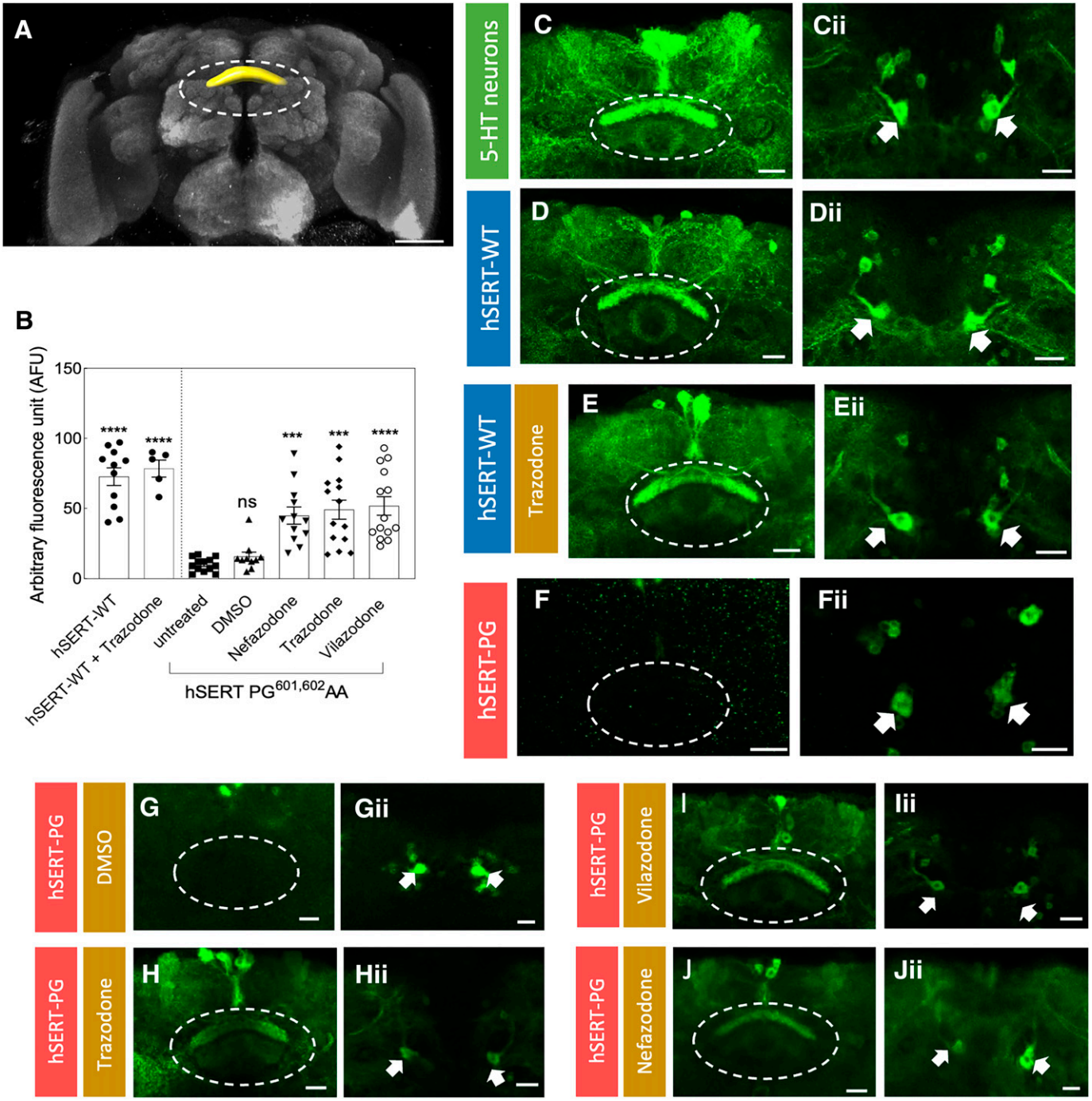

Fig. 11. Nefazodone, trazodone, and vilazodone restore presynaptic expression of folding-deficient hSERT-P601A/G 602A in the adult fly brain. (A) Schematic rendering of the adult fly brain highlighting the dorsal fan-shaped body (marked with yellow volume) and FB neuropil (dotted circle). (B) Quantification of the fluorescence signal in the dorsal FB region. Imaris 9.3 (Bitplane) was used to quantify the fluorescence signal in adult brains of each condition, i.e., flies expressing wild-type hSERT (n = 11), which received trazodone (n = 5), and flies expressing hSERT-P601A/G602A (hSERT-PG), which received control food (n = 13); food containing DMSO (n = 10); and food containing 100 μM each of trazodone (n = 12), vilazodone (n = 14), and nefazodone (n = 14) for 2 days. The statistical comparison was done by a Kruskal-Wallis test followed by Dunn's multiple comparison (****<0.0001 and ***<0.0002, significantly different from control or untreated flies); the P values for comparison versus untreated hSERT-P601A/G602A–expressing flies were 0.000001 for wild-type SERT, 1 for DMSO, 0.0006 for nefazodone, 0.0001 for trazodone, and 0.00004 for vilazodone. (C–J) and (Cii–Jii) display the corresponding, representative enlarged view of FB (dotted circle) and serotonergic cell bodies (arrows) innervating the FB, respectively. (C and Cii) The expression of membrane-anchored GFP in the distinct FB layers and corresponding serotonergic cell bodies, respectively. (D and Dii) Localization of YFP-tagged human wild-type serotonin transporter (hSERT-WT) in the FB neuropil and in cell bodies, respectively. (E and Eii) Localization of YFP-tagged hSERT-WT in the FB neuropil and in cell bodies, respectively, after treatment of flies for 48 hours with food containing 100 μM trazodone. (F–Iii) Localization of YFP-tagged human mutant SERT-P601A/G602A (hSERT-PG) in the FB neuropil (F–I) and cell bodies (Fii–Iii), respectively, in untreated male flies [only food (F and Fii); food containing DMSO (G and Gii)] or flies treated for 48 hours with food containing 100 μM each of trazodone (H and Hii), vilazodone (I and Iii), and nefazodone (J and Jii). Images from the brains of these flies were captured by confocal microscopy and compiled with the ImageJ software. Scale bars: (A) 50 μm, (C–Jii) 20 μm. Genotypes: (C and Cii) UAS-mCD8GFP, TRHT2A-GAL4; (D–Eii) UAS-YFP-hSERT-WT/TRHT2A-GAL4; (F–Iii) UAS-YFP-hSERT-PG 601,602 AA/TRHT2A-GAL4.

act as pharmacochaperones if they bind to the inward-facing conformation (El-Kasaby et al., 2010, 2014; Beerepoot et al., 2016; Kasture et al., 2016; Asjad et al., 2017; Bhat et al., 2017, 2020, 2023; Sutton et al., 2022). Here, we observed that the allosteric inhibitors nefazodone, trazodone, and vilazodone bound to the outward-facing state and were, nevertheless, effective pharmacochaperones. We therefore concluded that trapping of the nascent fold in the outward-facing conformation is per se not an obstacle to the folding trajectory. In fact, thermal inactivation shows that the inward- and outward-facing conformation are energetically equivalent stable folds (Ponleitner et al., 2022).

Electrophysiological recordings afford high temporal resolution: we relied on a protocol that allowed for monitoring binding events of low-affinity ligands in a label-free manner in real time (Hasenhuetl et al., 2015) to compare the binding kinetics of trazodone and vilazodone. The association and dissociation of trazodone were consistent with a simple bimolecular reaction. In contrast, we found that the interaction of vilazodone with SERT was governed by complex binding kinetics: an initial low-affinity binding event was followed by quasi-irreversible inhibition. Consistent with this observation, the potency of vilazodone in inhibiting substrate uptake depended on the incubation time: when added concomitantly with substrate, vilazodone inhibited substrate uptake with micromolar affinity, but a 15-minute preincubation enhanced the potency by about 200-fold. Similarly, the analysis of the pharmacochaperoning action (i.e., the restoration of substrate uptake by SERT-P601A/G602A) was hampered by the poor reversibility of vilazodone binding. The basis for the complex binding kinetics of vilazodone remains enigmatic. Clearly, a component is the lipophilicity of vilazodone and the resulting enrichment in the lipid phase: persistent inhibition by vilazodone was resistant to acid washes but partially reversible by washes with milk. We note that, in our experiments, vilazodone was a mixed-competitive inhibitor, whereas Plenge et al. (2021) reported noncompetitive inhibition. This discrepancy may be, in part, due to differences in preincubation time. In addition, molecular dynamics simulations indicate that vilazodone can also occupy the S1 site (Zhang et al., 2020). Entry into the S1 site can account for the mixed-competitive inhibition, which we observed for vilazodone and trazodone. We also note that vilazodone, nefazodone, and trazodone differed in their preference for the Na^+-bound state: this preference was more pronounced for trazodone (about ninefold) and vilazodone (about sixfold) than for nefazodone (about twofold). Thus, in spite of their common actions (i.e., as inhibitors of uptake and as pharmacochaperones), there must be subtle differences in their interaction with their binding site(s) in SERT.

The ideal pharmacochaperone ought to fulfill the following requirements: it must reach concentrations within the cell, which suffice to restore folding of its target. However, a pharmacochaperone must not cause persistent blockage of the rescued protein. It is difficult to predict the therapeutic potential of vilazodone because of its peculiar kinetics. In addition, vilazodone also has a long half-life (25 hours) (Schwartz et al., 2011). In contrast, trazodone has a short half-life (about 7 hours) and a volume of distribution of 0.84 L/kg (Nilsen and Dale, 1992), indicating that intracellular concentrations are in the same range as those in plasma. A therapeutic threshold concentration at steady state of 714 μg/L (about 1.9 μM) was defined for trazodone (Mihara et al., 2002). A peak concentration c_{max} in the range of 1500 μg/mL (about 4 μM) was achieved after administration of 100 mg trazodone (Kale and Agrawal, 2015). The concentration in the brain was estimated at 2800 μg/L (about 7.5 μM) after once-daily administration of 300 mg trazodone (Oggianu et al., 2022). The maximum approved doses of trazodone for outpatients and inpatients are 400 and 600 mg/day, respectively. Thus, therapeutic doses of trazodone reach concentrations where it is predicted to exert its pharmacochaperoning action. The same is true for nefazodone, which reaches peak concentrations of 2054 μg/L (= 4.4 μM) after administration of 200 mg (Barbhaiya et al., 1996) (the maximum approved dose is 600 mg/day). The half-life and the volume of distribution of nefazodone are 4 hours and 0.8 L/kg, respectively. Nefazodone elicited its pharmacochaperoning action with an EC_{50} of 2.5 μM. Thus, it is clear from our data that nefazodone exerts pharmacochaperoning actions at the concentrations that can be achieved in patients. In contrast, the pharmacochaperoning action of mCPP is of modest interest. Firstly, it was predictable: partial substrates are known to act as pharmacochaperones (Bhat et al., 2017, 2019). Secondly, mCPP was a low-efficacy and low-potency pharmacochaperone. Importantly, after administration of trazodone and nefazodone, plasma levels of mCPP are in the range of 0.3 μM (Greene and Barbhaiya, 1997; Otani et al., 1997) and thus substantially lower than those required for eliciting a pharmacochaperoning effect (EC_{50}, 15–25 μM). Several folding-deficient mutants of NET and DAT have been identified in people, and the phenotypic consequence has been linked to the resulting disease, but the role of folding-deficient variants of SERT is less well understood (Bhat et al., 2021a). Recently, two mutations of SERT (SERT-N217S and SERT-A500T) have been identified in treatment-resistant depression. The mutations have been proposed to cause a folding defect (J. F. Støier et al., preprint, DOI: 10.1101/2023.08.29.23294386). The pharmacochaperoning action of trazodone and nefazodone may be of therapeutic interest in these instances. This conjecture can be readily tested in affected individuals because trazodone and nefazodone are approved drugs.

Data Availability

The authors declare that all the data supporting the findings of this study are contained within the paper.

Authorship Contributions

Participated in research design: El-Kasaby, Kasture, Krumpl, Freissmuth, Sandtner.

Conducted experiments: El-Kasaby, Boytsov, Kasture.

Contributed new reagents or analytic tools: Hummel.

Performed data analysis: El-Kasaby, Boytsov, Kasture, Freissmuth, Sandtner.

Wrote or contributed to the writing of the manuscript: El-Kasaby, Kasture, Krumpl, Freissmuth, Sandtner.

References

Asjad HMM, Kasture A, El-Kasaby A, Sackel M, Hummel T, Freissmuth M, and Sucic S (2017) Pharmacochaperoning in a *Drosophila* model system rescues human dopamine transporter variants associated with infantile/juvenile parkinsonism. *J Biol Chem* **292**:19250–19265.

Baumann MH, Bulling S, Benaderet TS, Saha K, Ayestas MA, Partilla JS, Ali SF, Stockner T, Rothman RB, Sandtner W, et al. (2014) Evidence for a role of transporter-mediated currents in the depletion of brain serotonin induced by serotonin transporter substrates. *Neuropsychopharmacology* **39**:1355–1365.

Barbhaiya RH, Shukla UA, Chaikin P, Greene DS, and Marathe PH (1996) Nefazodone pharmacokinetics: assessment of nonlinearity, intra-subject variability and

time to attain steady-state plasma concentrations after dose escalation and de-escalation. *Eur J Clin Pharmacol* **50**:101–107.
Beerepoot P, Lam VM, and Salahpour A (2016) Pharmacological chaperones of the dopamine transporter rescue dopamine transporter deficiency syndrome mutations in heterologous cells. *J Biol Chem* **291**:22053–22062.
Bhat S, Hasenhuetl PS, Kasture A, El-Kasaby A, Baumann MH, Blough BE, Sucic S, Sandtner W, and Freissmuth M (2017) Conformational state interactions provide clues to the pharmacochaperone potential of serotonin transporter partial substrates. *J Biol Chem* **292**:16773–16786.
Bhat S, Newman AH, and Freissmuth M (2019) How to rescue misfolded SERT, DAT and NET: targeting conformational intermediates with atypical inhibitors and partial releasers. *Biochem Soc Trans* **47**:861–874.
Bhat S, Guthrie DA, Kasture A, El-Kasaby A, Cao J, Bonifazi A, Ku T, Giancola JB, Hummel T, Freissmuth M, et al. (2020) Tropane-based ibogaine analog rescues folding-deficient serotonin and dopamine transporters. *ACS Pharmacol Transl Sci* **4**:503–516.
Bhat S, El-Kasaby A, Freissmuth M, and Sucic S (2021a) Functional and biochemical consequences of disease variants in neurotransmitter transporters: a special emphasis on folding and trafficking deficits. *Pharmacol Ther* **222**:107785.
Bhat S, Niello M, Schicker K, Pifl C, Sitte HH, Freissmuth M, and Sandtner W (2021b) Handling of intracellular K^+ determines voltage dependence of plasmalemmal monoamine transporter function. *eLife* **10**:e67996.
Bhat S, El-Kasaby A, Kasture A, Boytsov D, Reichelt JB, Hummel T, Sucic S, Pifl C, Freissmuth M, and Sandtner W (2023) A mechanism of uncompetitive inhibition of the serotonin transporter. *eLife* **12**:e82641.
César-Razquin A, Snijder B, Frappier-Brinton T, Isserlin R, Gyimesi G, Bai X, Reithmeier RA, Hepworth D, Hediger MA, Edwards AM, et al. (2015) A call for systematic research on solute carriers. *Cell* **162**:478–487.
Coleman JA, Green EM, and Gouaux E (2016) X-ray structures and mechanism of the human serotonin transporter. *Nature* **532**:334–339.
Cusack B, Nelson A, and Richelson E (1994) Binding of antidepressants to human brain receptors: focus on newer generation compounds. *Psychopharmacology (Berl)* **114**:559–565.
Dawson LA and Watson JM (2009) Vilazodone: a 5-HT1A receptor agonist/serotonin transporter inhibitor for the treatment of affective disorders. *CNS Neurosci Ther* **15**:107–117.
El-Kasaby A, Just H, Malle E, Stolt-Bergner PC, Sitte HH, Freissmuth M, and Kudlacek O (2010) Mutations in the carboxyl-terminal SEC24 binding motif of the serotonin transporter impair folding of the transporter. *J Biol Chem* **285**:39201–39210.
El-Kasaby A, Koban F, Sitte HH, Freissmuth M, and Sucic S (2014) A cytosolic relay of heat shock proteins HSP70-1A and HSP90β monitors the folding trajectory of the serotonin transporter. *J Biol Chem* **289**:28987–29000.
Freissmuth M, Stockner T, and Sucic S (2018) SLC6 Transporter folding diseases and pharmacochaperoning. *Handb Exp Pharmacol* **245**:249–270.
Greene DS and Barbhaiya RH (1997) Clinical pharmacokinetics of nefazodone. *Clin Pharmacokinet* **33**:260–275.
Hasenhuetl PS, Schicker K, Koenig X, Li Y, Sarker S, Stockner T, Sucic S, Sitte HH, Freissmuth M, and Sandtner W (2015) Ligand selectivity among the dopamine and serotonin transporters specified by the forward binding reaction. *Mol Pharmacol* **88**:12–18.
Heinrich T, Böttcher H, Gericke R, Bartoszyk GD, Anzali S, Seyfried CA, Greiner HE, and Van Amsterdam C (2004) Synthesis and structure–activity relationship in a class of indolebutylpiperazines as dual 5-HT$_{(1A)}$ receptor agonists and serotonin reuptake inhibitors. *J Med Chem* **47**:4684–4692.
Hohenegger M, Mitterauer T, Voss T, Nanoff C, and Freissmuth M (1996) Thiophosphorylation of the G protein β subunit in human platelet membranes: evidence against a direct phosphate transfer reaction to G α subunits. *Mol Pharmacol* **49**:73–80.
Kale P and Agrawal YK (2015) Pharmacokinetics of single oral dose trazodone: a randomized, two-period, cross-over trial in healthy, adult, human volunteers under fed condition. *Front Pharmacol* **6**:224.
Kasture A, El-Kasaby A, Szöllősi D, Asjad HMM, Grimm A, Stockner T, Hummel T, Freissmuth M, and Sucic S (2016) Functional rescue of a misfolded *Drosophila melanogaster* dopamine transporter mutant associated with a sleepless phenotype by pharmacological chaperones. *J Biol Chem* **291**:20876–20890.
Kasture AS, Hummel T, Sucic S, and Freissmuth M (2018) Big lessons from tiny flies: *Drosophila melanogaster* as a model to explore dysfunction of dopaminergic and serotonergic neurotransmitter systems. *Int J Mol Sci* **19**:1788.
Koban F, El-Kasaby A, Häusler C, Stockner T, Simbrunner BM, Sitte HH, Freissmuth M, and Sucic S (2015) A salt bridge linking the first intracellular loop with the C terminus facilitates the folding of the serotonin transporter. *J Biol Chem* **290**:13263–13278.
Koban F and Freissmuth M (2023) The cell cycle protein MAD2 facilitates endocytosis of the serotonin transporter in the neuronal soma. *EMBO Rep* **24**:e53408.
Korkhov VM, Holy M, Freissmuth M, and Sitte HH (2006) The conserved glutamate (Glu136) in transmembrane domain 2 of the serotonin transporter is required for the conformational switch in the transport cycle. *J Biol Chem* **281**:13439–13448.
Krege S, Goepel M, Sperling H, and Michel MC (2000) Affinity of trazodone for human penile α1- andalpha2-adrenoceptors. *BJU Int* **85**:959–961.
Kusek J, Yang Q, Witek M, Gruber CW, Nanoff C, and Freissmuth M (2015) Chaperoning of the A1-adenosine receptor by endogenous adenosine - an extension of the retaliatory metabolite concept. *Mol Pharmacol* **87**:39–51.
Li M, Chen Q, and Zhang YW (2022) Determining ligand and ion-induced conformational changes in serotonin transporter with its fluorescent substrates. *Int J Mol Sci* **23**:10919.
Marinko JT, Huang H, Penn WD, Capra JA, Schlebach JP, and Sanders CR (2019) Folding and misfolding of human membrane proteins in health and disease: from single molecules to cellular proteostasis. *Chem Rev* **119**:5537–5606.
Mihara K, Yasui-Furukori N, Kondo T, Ishida M, Ono S, Ohkubo T, Osanai T, Sugawara K, Otani K, and Kaneko S (2002) Relationship between plasma concentrations of trazodone and its active metabolite, m-chlorophenylpiperazine, and its clinical effect in depressed patients. *Ther Drug Monit* **24**:563–566.
Nilsen OG and Dale O (1992) Single dose pharmacokinetics of trazodone in healthy subjects. *Pharmacol Toxicol* **71**:150–153.
Oggianu L, Di Dato G, Mangano G, Rosignoli MT, McFeely S, Ke AB, Jones HM, and Comandini A (2022) Estimation of brain receptor occupancy for trazodone immediate release and once a day formulations. *Clin Transl Sci* **15**:1417–1429.
Ok SH, Hong JM, Lee SH, and Sohn JT (2018) Lipid emulsion for treating local anesthetic systemic toxicity. *Int J Med Sci* **15**:713–722.
Otani K, Mihara K, Yasui N, Ishida M, Kondo T, Tokinaga N, Ohkubo T, Osanai T, Sugawara K, and Kaneko S (1997) Plasma concentrations of trazodone and m-chlorophenylpiperazine at steady state can be predicted from those after an initial dose of trazodone. *Prog Neuropsychopharmacol Biol Psychiatry* **21**:239–244.
Owens MJ, Morgan WN, Plott SJ, and Nemeroff CB (1997) Neurotransmitter receptor and transporter binding profile of antidepressants and their metabolites. *J Pharmacol Exp Ther* **283**:1305–1322.
Plenge P, Yang D, Salomon K, Laursen L, Kalenderoglou IE, Newman AH, Gouaux E, Coleman JA, and Loland CJ (2021) The antidepressant drug vilazodone is an allosteric inhibitor of the serotonin transporter. *Nat Commun* **12**:5063.
Ponleitner M, Szöllősi D, El-Kasaby A, Koban F, Freissmuth M, and Stockner T (2022) Thermal unfolding of the human serotonin transporter: differential effect by stabilizing and destabilizing mutations and cholesterol on thermodynamic and kinetic stability. *Mol Pharmacol* **101**:95–105.
Sahni N, Yi S, Taipale M, Fuxman Bass JI, Coulombe-Huntington J, Yang F, Peng J, Weile J, Karras GI, Wang Y, et al. (2015) Widespread macromolecular interaction perturbations in human genetic disorders. *Cell* **161**:647–660.
Schicker K, Uzelac Z, Gesmonde J, Bulling S, Stockner T, Freissmuth M, Boehm S, Rudnick G, Sitte HH, and Sandtner W (2012) Unifying concept of serotonin transporter-associated currents. *J Biol Chem* **287**:438–445.
Schlessinger A, Zatorski N, Hutchinson K, and Colas C (2023) Targeting SLC transporters: small molecules as modulators and therapeutic opportunities. *Trends Biochem Sci* **48**:801–814.
Schwartz TL, Siddiqui UA, and Stahl SM (2011) Vilazodone: a brief pharmacological and clinical review of the novel serotonin partial agonist and reuptake inhibitor. *Ther Adv Psychopharmacol* **1**:81–87.
Segel IH (1975) *Enzyme Kinetics: Behaviour and Analysis of Rapid Equilibrium and Steady-State Enzyme Systems*, John Wiley & Sons Inc., Hoboken, New Jersey.
Sitte HH and Freissmuth M (2015) Amphetamines, new psychoactive drugs and the monoamine transporter cycle. *Trends Pharmacol Sci* **36**:41–50.
Sucic S, El-Kasaby A, Kudlacek O, Sarker S, Sitte HH, Marin P, and Freissmuth M (2011) The serotonin transporter is an exclusive client of the coat protein complex II (COPII) component SEC24C. *J Biol Chem* **286**:16482–16490.
Sucic S, Koban F, El-Kasaby A, Kudlacek O, Stockner T, Sitte HH, and Freissmuth M (2013) Switching the clientele: a lysine residing in the C terminus of the serotonin transporter specifies its preference for the coat protein complex II component SEC24C. *J Biol Chem* **288**:5330–5341.
Sutton C, Williams EQ, Homsi H, Beerepoot P, Nazari R, Han D, Ramsey AJ, Mash DC, Olson DE, Blough B, et al. (2022) Structure-activity relationships of dopamine transporter pharmacological chaperones. *Front Cell Neurosci* **16**:832536.
Tatsumi M, Groshan K, Blakely RD, and Richelson E (1997) Pharmacological profile of antidepressants and related compounds at human monoamine transporters. *Eur J Pharmacol* **340**:249–258.
Zhang Y, Zheng G, Fu T, Hong J, Li F, Yao X, Xue W, and Zhu F (2020) The binding mode of vilazodone in the human serotonin transporter elucidated by ligand docking and molecular dynamics simulations. *Phys Chem Chem Phys* **22**:5132–5144.
Zhu R, Sinwel D, Hasenhuetl PS, Saha K, Kumar V, Zhang P, Rankl C, Holy M, Sucic S, Kudlacek O, et al. (2016) Nanopharmacological force sensing to reveal allosteric coupling in transporter binding sites. *Angew Chem Int Ed Engl* **55**:1719–1722.

Address correspondence to: Michael Freissmuth, Institute of Pharmacology and the Gaston H. Glock Research Laboratories for Exploratory Drug Development, Centre of Physiology and Pharmacology, Medical University of Vienna, Vienna, Waehringerstrasse 13a, Vienna, 1090, Austria. E-mail: michael.freissmuth@meduniwien.ac.at